https://ntrs.nasa.gov/search.jsp?R=19720004927 2020-03-11T21:54:19+00:00Z

CR- 123266

TM-71-1022-3

TECHNICAL MEMORANDUM

THE QUASI-INERTIAL AND WIDE-DEADBAND MODES AS BACKUP ATTITUDE OPTIONS FOR THE SKYLAB MISSION

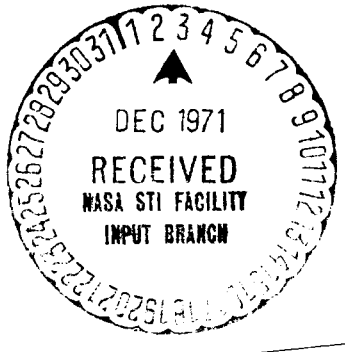

Bellcomm

N72-12576 (NASA-CR-123266) THE QUASI-INERTIAL AND WIDE-DEADBAND MODES AS BACKUP ATTITUDE OPTIONS FOR THE SKYLAB MISSION B.D. Elrod (Bellcomm, Inc.) 19 Jun. 1971 71 P

Unclas 09242 CSCL 17G G3/21

FAC (NASA CR OR TMX OR AD NUMBER) (CATEGORY)

BELLCOMM, INC.
955 L'ENFANT PLAZA NORTH, S.W., WASHINGTON, D.C. 20024

COVER SHEET FOR TECHNICAL MEMORANDUM

TITLE- The Quasi-Inertial and Wide-Deadband Modes as Backup Attitude Options for the Skylab Mission

TM- 71-1022-3

DATE- June 19, 1971

FILING CASE NO(S)- 620

AUTHOR(S)- B. D. Elrod

FILING SUBJECT(S) (ASSIGNED BY AUTHOR(S))- Skylab Program
Spacecraft Attitude Control
Reaction Thrust Systems
Solar Orientation

ABSTRACT

The Quasi-Inertial (QI) and Wide-Deadband (WDB) modes have been investigated as alternatives to the Solar-Inertial (SI) mode in case two CMGs fail during the Skylab mission. Both modes provide a substantial reduction in propellant requirements from the solar inertial hold requirement with either the Orbital Assembly/Thruster Attitude Control System (OA/TACS) or Service Module/Reaction Control System (SM/RCS). Spacecraft motion in the QI mode is produced by a command rate and results in a small amplitude oscillation (17°, maximum) about the SI orientation. In the WDB mode a somewhat similar, but larger amplitude motion (35°, maximum) about the SI orientation is developed by appropriate choice of controller deadbands and switch line slopes.

In the QI mode the potential mission duration is 45 days with the OA/TACS and 56 days with the SM/RCS. This compares with 24 days and 28 days in the WDB mode and 3-4 days in the SI mode. With SM/RCS control in the QI mode during CSM visits and OA/TACS control during the storage period it is conceivable that both SL-3 and SL-4 segments of the Skylab mission could be completed even if 2 CMGs fail near the SL-3 launch.

Besides the longer potential mission duration other performance factors stand out in favor of the QI mode. Specifically, the electrical energy output from the solar arrays is essentially identical to the SI mode and opportunities for solar viewing with the ATM range from 10-28% of the time available in the SI mode. Correspondingly, the loss in electrical energy output is 10-12% in the WDB mode and ATM solar viewing opportunities are negligible.

Implementation of the QI mode with the OA/TACS or SM/RCS does require a software modification to generate the command rate. Implementation of the WDB mode with the OA/TACS requires only occasional uplinking of control law parameters. However, a significant modification is required for the SM/RCS to permit independent selection of deadbands and switch line slopes in the CSM Digital Autopilot (DAP) for all control axes.

BA-145A (8-68)

SEE REVERSE SIDE FOR DISTRIBUTION LIST

DISTRIBUTION

COMPLETE MEMORANDUM TO

CORRESPONDENCE FILES:

OFFICIAL FILE COPY
plus one white copy for each additional case referenced

TECHNICAL LIBRARY (4)

NASA Headquarters

H. Cohen/MLR
J. H. Disher/MLD
W. B. Evans/MLO
W. H. Hamby/MLO
T. E. Hanes/MLA
A. S. Lyman/MR
M. Savage/MLT
W. C. Schneider/ML

MSC

A. A. Bishop/KA
C. Conrad/CB
K. J. Cox/EG23
R. W. Cunningham/CB
F. M. Elam/EG25
O. K. Garriott/CB
K. S. Kleinknecht/PA
W. J. Klinar/EG13
T. P. Lins/EG2
F. C. Littleton/KM
P. C. Shaffer/KA
O. G. Smith/KW
H. W. Tindall/FA
H. E. Whitacre/KM

MSFC

J. F. Applegate/S&E-ASTR-SGD
L. F. Belew/PM-AA-MGR
W. B. Chubb/S&E-ASTR-SGD
G. B. Hardy/PM-AA-EI
H. F. Kennel/S&E-ASTR-A
S. R. Reinartz/PM-AA-MGR
C. C. Rupp/S&E-ASTR-SGA
R. G. Smith/PM-SAT-MGR
R. E. Tinius/S&E-CSE-AM
H. E. Worley/S&E-AERO-DO

BA-146 (8-64)

COMPLETE MEMORANDUM TO (CONTINUED)

Delco Electronics

E. O. Shika

LaRC

W. W. Anderson/AMPD
P. R. Kurzhals/AMPD

Martin-Marietta/Denver

F. Bickley
W. Cain
T. Glahn
C. Rybak

McDonnell Douglas/East

R. Glowczwski

MIT - Charles Stark Draper Lab.

S. Copps/23C
G. Stubbs/23C
J. Turnbull/23C

TRW/Houston

R. D. Miller
F. W. Polaski
R. W. Rountree
T. J. Smith
E. V. Thatcher

Bellcomm

A. P. Boysen
J. P. Downs
J. J. Fearnsides
D. R. Hagner
W. G. Heffron
D. P. Ling
J. Z. Menard
J. M. Nervik
E. A. Nussbaumer
P. F. Sennewald
W. B. Thompson
J. W. Timko
R. L. Wagner
R. A. Wenglarz
M. P. Wilson
Departments 1013, 2013, 2031 Supervis
Departments 1022, 1024, 1025
Department 1024 File
Central File

Table of Contents

Bellcomm

955 L'Enfant Plaza North, S.W.
Washington, D. C. 20024

date: June 19, 1971

to: Distribution

from: B. D. Elrod

TM-71-1022-3

subject: The Quasi-Inertial and Wide-Deadband Modes as Backup Attitude Options for the Skylab Mission - Case 620

TECHNICAL MEMORANDUM

1.0 Introduction

As currently planned, the Skylab mission will be conducted with the Orbital Assembly (OA) in the solar inertial (SI) mode* except for docking operations and those orbits when earth resources experiments will be performed in a local vertical orientation. Attitude control of the Skylab will be provided primarily by three control moment gyros (CMGs). Additional control capability is available from the Orbital Assembly/Thruster Attitude Control System (OA/TACS) and the Service Module/Reaction Control System (SM/RCS) for performing certain docking and momentum management operations and to counteract venting torques.

Because the Skylab mission spans a period of nearly 8 months, the question of backup attitude modes is of interest in the event that two or more CMGs fail. Holding the solar inertial orientation with the TACS or RCS would impose a prohibitive drain on reaction thrust propellant and force early curtailment of the mission. The objective of this memorandum is to describe two possible alternative modes in which a nominal solar orientation is maintained with relatively low propellant impulse requirements.

The backup options are termed: the Quasi-Inertial (QI) mode and the Wide-Deadband (WBD) mode. While conceptually related in terms of the resultant spacecraft motion, they differ in the manner of control implementation. In the QI mode a rate

---

*The SI mode is defined[1] by the orientation of OA geometric axes (x_v, y_v, z_v): z_v (normal to solar array) is pointed to the sun and x_v is rotated (about z_v) an angle ν_z from the orbital plane. Nominally ν_z is such that the x principal axis lies in the orbital plane.

command is utilized with tight limit cycle control to cause the x principal axis of the OA to oscillate in the orbital plane with the solar arrays pointed (nominally) to the sun. In the WDB mode a somewhat similar motion is developed without command rate by appropriate choice of TACS or RCS control law parameters (deadband and switch line slope).

Further description of each mode is given in the next two sections. Impulse requirements for maintaining each mode are compared with that for the SI mode in Section 4. The question of attitude updating is discussed in Section 5. The appendices contain an analytical treatment of the QI mode from a more general viewpoint than in an earlier memorandum.[2]

2.0 The Quasi-Inertial Mode

The QI Mode can be described in terms of the motion of spacecraft principal axes (x_p, y_p, z_p) relative to orbital coordinates (x_N, y_N, z_N) shown in Figure 1a. In this system z_N is the orbit normal and x_N is parallel to the intersection of the orbit and noon meridian planes. The principal axis x_p lies in the orbital plane with an instantaneous angular displacement Ψ relative to x_N. The y_p and z_p principal axes are rotated about x_p by a fixed, but arbitrary, displacement, Φ_o, as shown in Figure 1a. The QI motion is such that x_p oscillates about a nominal orientation Ψ_N, which can be chosen arbitrarily.

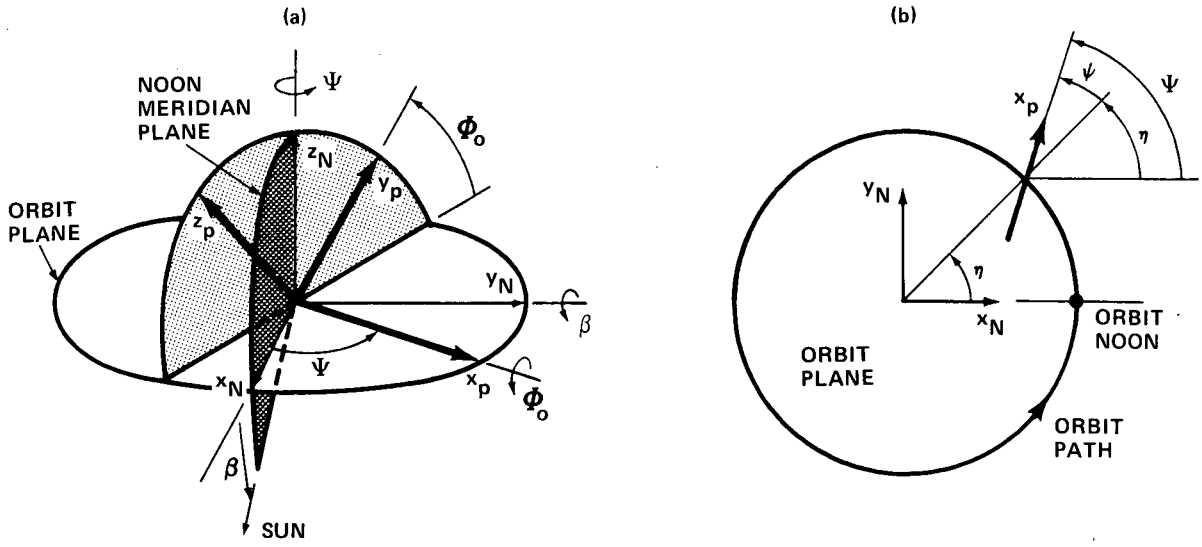

FIGURE 1 - ORIENTATION OF SPACECRAFT PRINCIPAL AXES IN QUASI-INERTIAL MODE

2.1 Analytical Description

In Appendix A.1 a general mathematical representation of the QI motion is developed based on the differential equation

$$\ddot{\Psi} = -\frac{3\Omega_o^2}{2}\hat{K}\sin 2(\Psi-\eta) \tag{1}$$

which describes motion of the x_p axis in the orbital plane. Here Ω_o is the orbit angular velocity, $\hat{K}$ is an arbitrary constant to be specified and η is orbital position measured relative to orbital noon. Another form of Eq. (1) analogous to the differential equation for motion of a simple pendulum is

$$\ddot{\psi} = -\frac{3\Omega_o^2}{2}\hat{K}\sin 2\psi = -B\sin 2\psi \tag{2}$$

where*

$$\psi \equiv \Psi - \eta = \Psi - \Omega_o(t-t_n) \tag{3}$$

is the instantaneous angular displacement of x_p from local vertical. See Figure 1b.

If the motion Ψ is to be periodic, it is necessary that the average value of $\dot{\Psi}$ be zero, so from Eq. (3)

$$\dot{\psi}_{ave} = \dot{\Psi}_{ave} - \Omega_o = -\Omega_o < 0 \tag{4}$$

This means that the motion $\psi(t)$ corresponding to Eq. (2) must include a secular component representing continuous rotation of x_p relative to local vertical once per orbit. The resultant motion is analogous to that of a pendulum spinning about its pivot.

---

*A circular orbit is assumed so that $\eta=\Omega_o(t-t_n)$ where t is absolute time and t_n is absolute time at last orbital noon.

The periodic motion of x_p about the nominal orientation (Ψ_N) can be expressed in terms of ψ as*

$$\Delta\Psi \equiv \Psi - \Psi_N = \psi - (k/\lambda) F(k,\psi) \tag{5}$$

$$\Delta\dot{\Psi} = \dot{\Psi} = \dot{\psi} + \Omega_o$$

$$= \Omega_o \left(1 - \frac{\lambda}{k}\sqrt{1-k^2\sin^2\psi}\right) \tag{6}$$

where

$$\lambda \equiv \sqrt{3\hat{K}} \tag{7}$$

and k is a constant of integration chosen to satisfy the oscillation condition*

$$\frac{\pi}{2}\lambda = k\,K(k) \tag{8}$$

which results from Eq. (4). The terms $K(k)$ and $F(k,\psi)$ are complete and incomplete elliptic integrals of the first kind. The nominal orientation (Ψ_N) is related to $\psi(t_n) \equiv \psi_n$ by

$$\Psi_N \equiv (k/\lambda) F(k,\psi_n) \tag{9}$$

The oscillation amplitude ($\Delta\Psi_m$) is given by

$$\Delta\Psi_m \equiv |\Psi_m - \Psi_N| = \psi_m - (k/\lambda)\, F(k,\psi_m) \tag{10}$$

where

$$\psi_m \equiv \sin^{-1}\sqrt{1/k^2 - 1/\lambda^2} \tag{11}$$

---

*See Eqs. (15) - (21) in Appendix A-1 and Footnote * on p. A-5.

The relationship of the QI motion ($\Psi-\Psi_N$) to the quantities ψ and $\hat{K}$ is depicted in Figure 2. In Appendix A-4 an optimal $\hat{K}$ is found in terms of spacecraft inertia parameters, which minimizes the control impulse requirements for maintaining the QI mode. In fact, if the spacecraft is symmetrical ($I_z=I_y$), or if two principal axes lie in the orbital plane ($\Phi_o=0, \pm\pi/2, \pm\pi$), a $\hat{K}$ exists for which no control is required theoretically, that is, the QI motion is a natural motion of the spacecraft. Since the optimal $|\hat{K}|$ turns out to be ≤ 1 in any case, only the range $0 \leq |\hat{K}| \leq 1$ is shown in Figure 2. Note that $\hat{K} = 0$ corresponds to an inertial orientation.* For a specific $\hat{K}$ the oscillation variables ($\Delta\Psi, \Delta\dot{\Psi}$) can be evaluated from Eqs. (5) and (6) as a function of time after integrating the differential equation**

$$\dot{\psi} = -\Omega_o(\lambda/k)\sqrt{1-k^2\sin^2\psi} \qquad (12)$$

for $\psi(t)$ with the initial condition ψ_n, which is related to Ψ_N by Eq. (8).***

Since Φ_o and Ψ_N are arbitrary, a given spacecraft axis can be pointed arbitrarily in the celestial sphere. Because the oscillation amplitude ($\Delta\Psi_m$) is low it will remain within a small neighborhood of the nominal orientation. As determined in Appendix A-2 the maximum deviation from the nominal is $\Delta\Psi_m$, if this axis lies in the orbital plane, and this decreases with increasing latitude of the axis relative to the orbital plane.

---

*See Footnote**, p. A-7.

**See Eq. (6).

***Other initial conditions for ψ are discussed in Section 5.3.

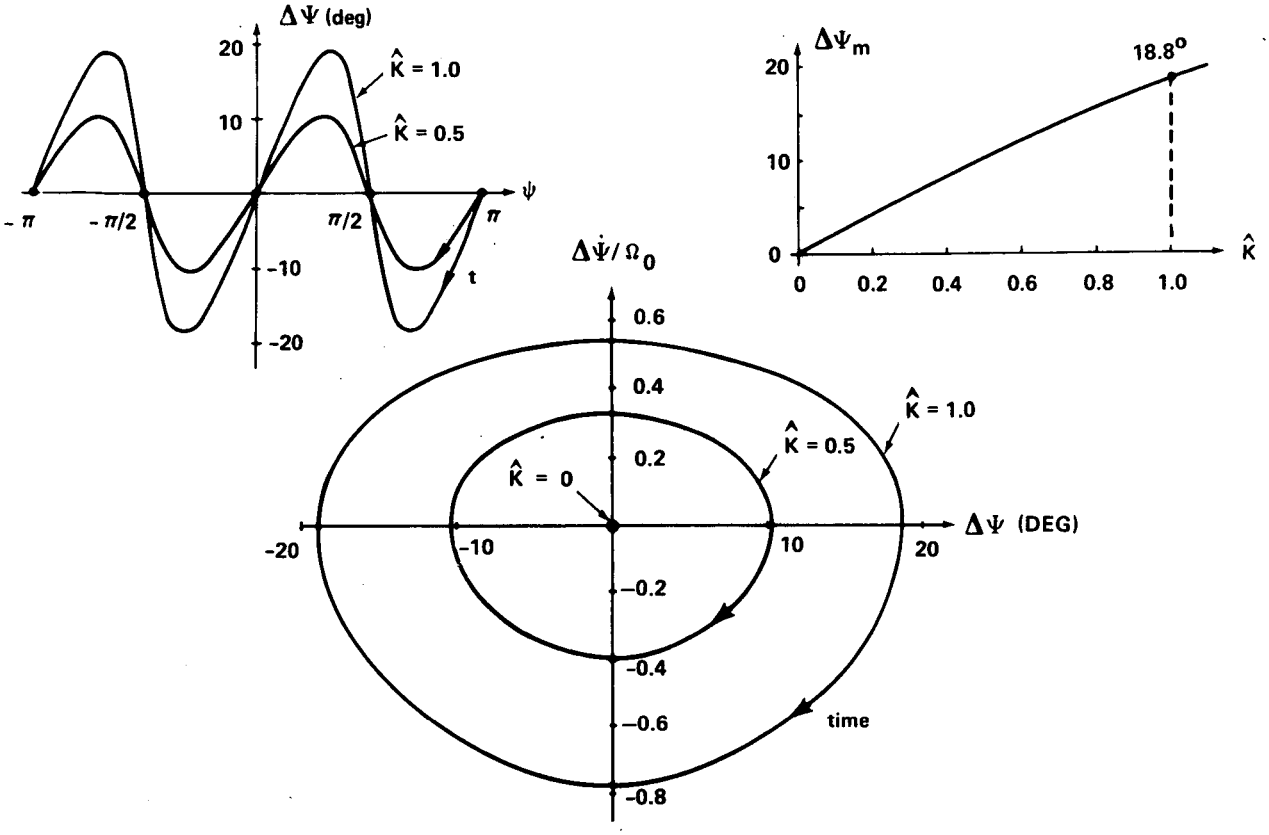

FIGURE 2 - RELATIONSHIP OF QI MOTION TO ψ AND $\hat{K}$

2.2 Skylab Application

Attitude control of the Skylab OA in the QI mode with the OA/TACS or CSM/RCS requires specification of a command rate, $\dot{\underline{\theta}}_C$, for use in generating appropriate control torque.* From the previous discussion it is clear that $\dot{\underline{\theta}}_C$ is a vector parallel to the orbit normal and can be expressed as

$$\dot{\underline{\theta}}_C = \begin{pmatrix} 0 \\ 0 \\ \dot{\psi} \end{pmatrix} \tag{13}$$

*Note the discussion in Appendix A.2, p. A-7.

in (x_N, y_N, z_N) coordinates shown in Figure 1. On-board evaluation of $\dot{\underline{\Theta}}_c$ entails calculation of $\dot{\Psi}$ from Eq. (6) with ψ obtained by numerical integration of Eq. (12) with an initial condition ψ_o based on Ψ_N. Updating of ψ_o based on sensor data and certain navigation computations is discussed in Section 5. Propellant impulse requirements for maintaining the QI mode are discussed in Section 4 and Appendix A.4.

The primary attitude mode during the Skylab mission is the solar inertial mode.* A nominal solar orientation can be obtained in the QI mode by specifying Φ_o and Ψ_N such that the Skylab z geometric axis (z_v - normal to solar arrays) nominally points to the sun. Both Φ_o and Ψ_N must be updated at intervals, since β, the minimum angle between the sun line and the orbital plane,** varies slowly with time. From the results in Appendix A.3 and Figure (A-5) it is apparent that $0° \leq \Phi_o \leq 147°$ and $93.8° \leq \Psi_N \leq 103.8°$, since $|\beta| \leq 73.5°$ during the Skylab mission.

The deviation of z_v from the sunline due to the QI motion is given in Eq. (A-35) as

$$\delta_{zv} = \cos^{-1}[\cos^2\beta \cos(\Psi-\Psi_N) + \sin^2\beta] \qquad (14)$$

The maximum possible deviation which occurs at $\beta=0°$ is $\Delta\Psi_m$, the oscillation amplitude. For the Skylab configuration $\Delta\Psi_m$ is in the range $16.2° \leq \Delta\Psi_m \leq 16.6°$ depending on the choice of $\hat{K}$ ***, so that $\delta_{zv} \leq 16.6°$.

Performance of the solar array system should be relatively insensitive to the QI motion. The maximum instantaneous cosine loss in electrical power from the arrays is 4%. However, the average of

---

*See Footnote *, p. 1.

**See Figure (A-5), p. A-11.

***See Section 4 and Appendix A.4 regarding the choice of $\hat{K}$.

cos δ_{zv} over an orbit sun-light interval exceeds 0.995 in the worst case (β=0°), which amounts to a 0.5% average energy loss (maximum).

Use of the ATM for solar observations in the QI mode is a possibility during intervals when the angular deviation δ_{zv} is within ATM gimbal limits. Had the ATM yaw gimbal range been designed to exceed $\pm\Delta\Psi_m$, full use of the ATM could be achieved, since $\delta_{zv} \leq \Delta\Psi_m$. Because of the present gimbal limits ($\delta_G = \pm 2°$)[5] the interval during which the sun is within view is restricted to certain orbital sectors as shown in Figure 3a.* The intervals are smallest at β=0° and increase with $|\beta|$ according to the relation

$$\hat{\eta} = \sin^{-1}\left(\frac{\cos^{-1}\left(\frac{\cos\delta_G - \sin^2\beta}{\cos^2\beta}\right)}{\Delta\Psi_m}\right) \qquad (15)$$

The sector near orbital midnight becomes available for high $|\beta|$ as the earth shadow interval disappears. The angular sum (η_T) of the sectors is plotted vs β in Figure 3b for $\Delta\Psi_m$=16.6° and $|\delta_G|$=2° and 6°. At $|\beta|_{max}$=73.5°, four 25° sectors are available for ATM solar observations. The 6° curve will be of interest, since it is equivalent to the interval during which the acquisition sun sensor operates in the linear range ($\pm$6°). This is of use in attitude updating as discussed in Section 5.

3.0 The Wide-Deadband Mode

The WDB mode is a means for obtaining an approximately periodic spacecraft motion relative to a solar inertial orientation. The approach involves selecting the drift zone characteristics of the reaction thrust controller (TACS or RCS deadband and switch line slope) to encourage a limit cycle motion with attitude "turning points" established primarily by environmental torques (essentially gravity-gradient torque). The resultant motion is similar to the QI motion but never synchronizes to it

---

*The axis z_v is parallel to the sun line (δ_{zv}=0°) at the center of each sector (located at $\eta=\Psi_N \pm m\pi/2$, m=0,1,2).

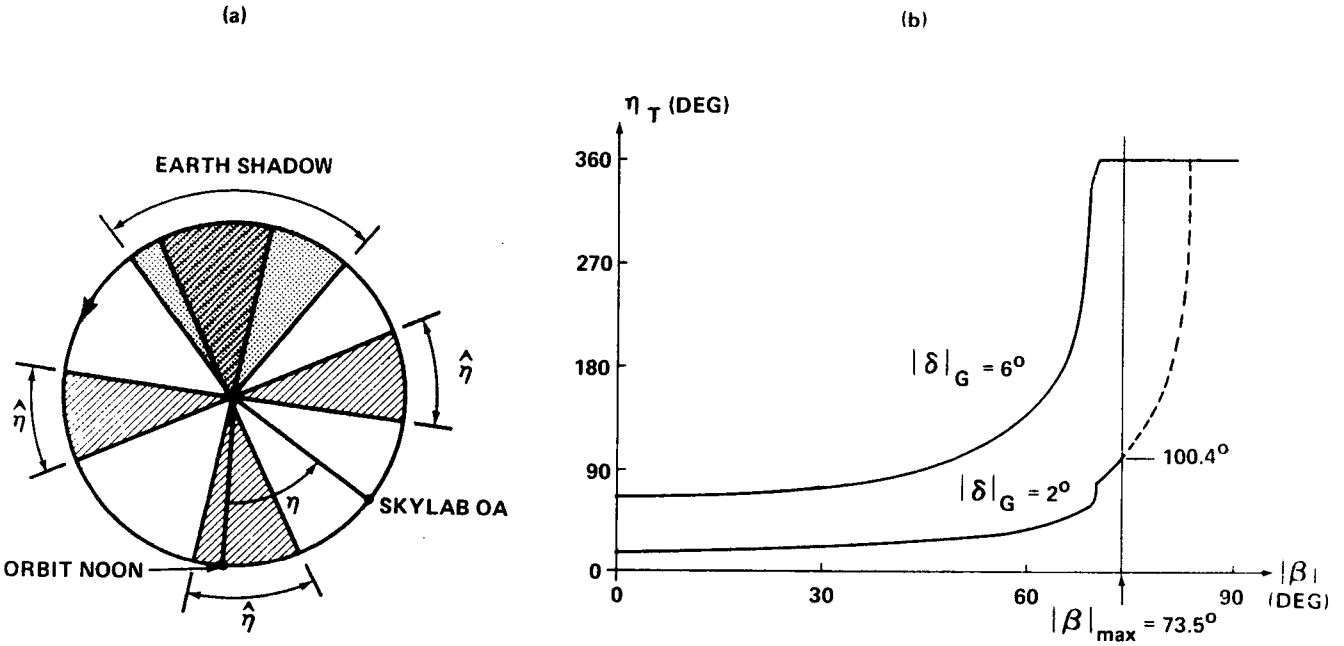

FIGURE 3 - EFFECT OF β ON ORBIT SECTOR ANGLE FOR ATM SOLAR VISIBILITY IN QI MODE

because no command rate is used. This concept was originally investigated in connection with x axis control of the "Wet Workshop" in the X-POP mode.*[7,8] The control requirement in the Skylab application is somewhat more complex however, since the desired nominal SWS attitude is the solar inertial orientation, which changes with β. In the following a rationale is described for selecting the control law parameters (deadband and switch line slope) as a function of β.

Controller characteristics for a particular control axis are represented in this discussion by the phase-plane diagram shown in Figure 4a. This is based on the usual position-plus-rate feedback control law

---

*In this mode the x_v axis is perpendicular to the orbital plane.

$$E = A_0 \phi_e + A_1 \dot{\phi}_e \tag{15}$$

which results in a thruster firing whenever $|E|>1$, that is, whenever the attitude and rate error statepoint $(\phi_e, \dot{\phi}_e)$ lies outside the drift zone. The attitude deadband is specified by $\pm 1/A_0$ and the switch line slope by $-A_0/A_1$.

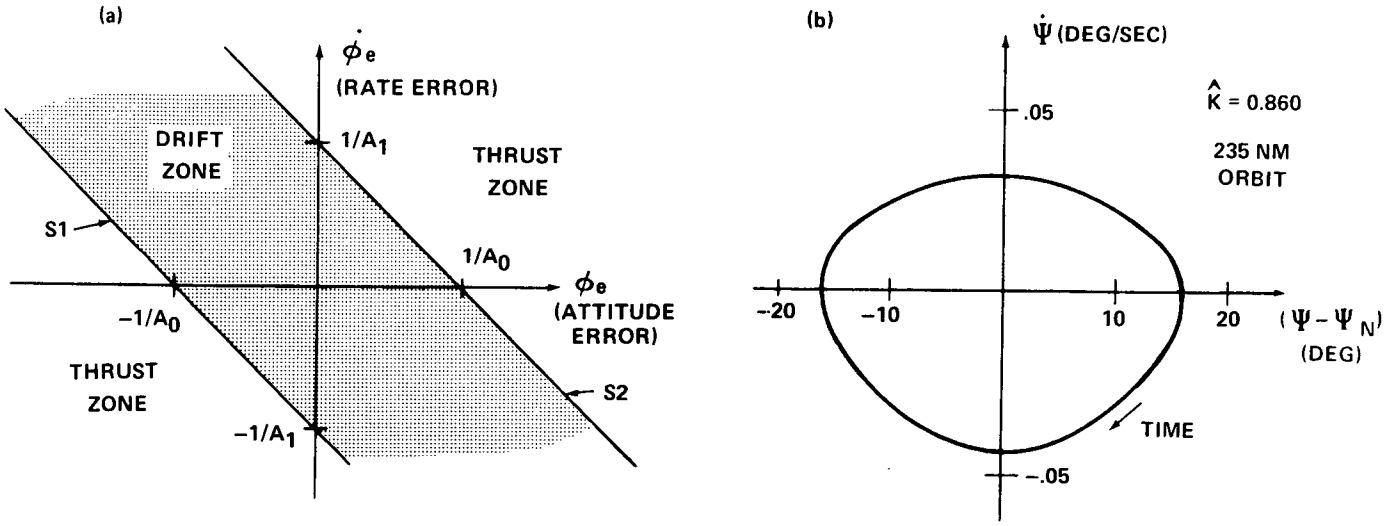

FIGURE 4 - CONTROLLER PHASE PLANE DIAGRAM AND QI MODE PHASE TRAJECTORY

Some insight into selecting the parameters A_0 and A_1 can be gained from the phase plane trajectory shown in Figure 4b corresponding to the OA in the QI mode. Suppose for example that the OA control axis y_v is a principal axis oriented normal to the orbital plane and that only gravity-gradient torque acts on the spacecraft. Then a natural limit cycle* can be established about

*A limit cycle motion without thruster firings is termed a natural limit cycle or free oscillation.

this axis with proper initialization ($\dot{\phi}_{eo}=\dot{\Psi}_o$, $\phi_{eo}=\Psi_o-\Psi_N$) and the drift zone adjusted such that the QI phase trajectory lies between the switch lines (S1,S2) in Figure 4a. This implies that the average angular rate ($\dot{\phi}_{e\ ave}$) over an orbit remains zero. Because of imperfect initialization, environmental and operational disturbances (e.g. aerodynamic torque, spacecraft venting), a zero average rate is unlikely in the absence of a command rate. Hence the phase trajectory tends to drift right or left in helix fashion eventually intersecting a switch line with a resultant thruster firing.

Nearly vertical switch lines, even though bounding the idealized phase trajectory, represent a hard deadband and yield only a slight reduction in propellant consumption from the solar inertial hold requirement. Horizontal switch lines, on the other hand, provide no average inertial hold (due to the helix type motion). Positioning switch lines nearly tangent to the idealized phase trajectory near $\phi_e=0$ as in Figure 5a leads to a reasonable compromise between attitude deviations and propellant consumption. This switch line arrangement provides a rate limiting effect with attitude

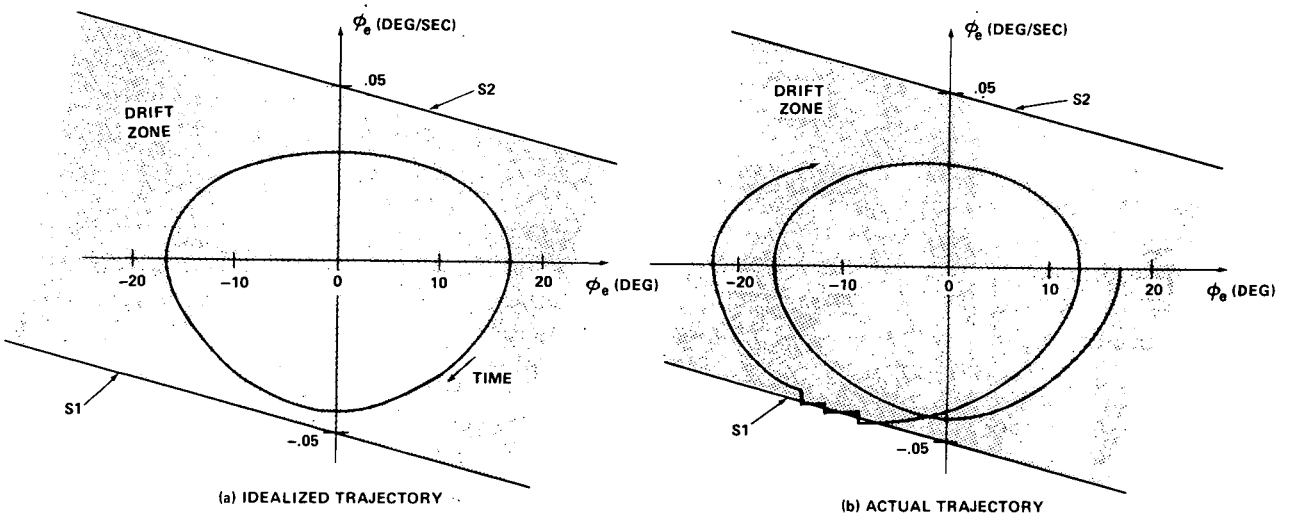

FIGURE 5 - ACTUAL AND IDEALIZED PHASE TRAJECTORIES ON CONTROLLER PHASE PLANE DIAGRAM IN WDB MODE

"turning points" ($\dot{\phi}_e$=0) produced naturally by gravity-gradient torque. As observed in computer simulations and illustrated in Figure 5b, the resultant phase trajectory has an oscillatory character much like the idealized trajectory, but drifts within the dead-zone, intersects the switch line drifts back, etc.

Usually a principal axis would not be normal to the orbital plane and furthermore control axes (x_v,y_v,z_v) are generally displaced from principal axes (x_p,y_p,z_p). If the idealized (QI) motion were to be established,* a component of the motion would appear about all three control axes. The components of the motion viewed about the OA x_v, y_v and z_v axes are shown in Figure 6 for several values of β.** Nonetheless the foregoing discussion regarding controller parameter selection can still be based on the idealized motion with a slight modification. That is, deadband and switch line slope for any particular control axis need only be adjusted to accommodate the component motion. With no claim to optimality, the control parameters (A_0,A_1) plotted in Figure 7 have been found in simulation studies of TACS control of the OA to provide a significant reduction in propellant consumption compared to the solar inertial hold requirement.*** The x axis control parameters were found to be relatively insensitive to changes in β and were maintained constant as indicated in Figure 7.

While deadbands ($\pm 1/A_0$) as large as $\pm$50° are indicated, maximum attitude deviations of only $\pm$30°-35° are typical due to natural "turning points" occurring well below the deadband limit. The resultant spacecraft motion is such that the z_v axis oscillates about the sun line somewhat like in the QI mode, but with a larger amplitude. A typical variation of the solar pointing error (angle between z_v and the sun line) is shown in Figure 13 (Section 5).

---

*If a principal axis (y_p or z_p) is not normal to the orbital plane, the QI motion is not strictly a natural motion since some control torque (although small) is required to sustain it. (See Appendix A.4).

**Resolution of components is based on Skylab OA mass properties data.[4] Since x_v and x_p axes are nearly coincident ($\sim$3.8° displacement), the component of motion about the x_v axis is very small (2°, maximum displacement at high β).

***Numerical results on propellant requirements are given in the next section.

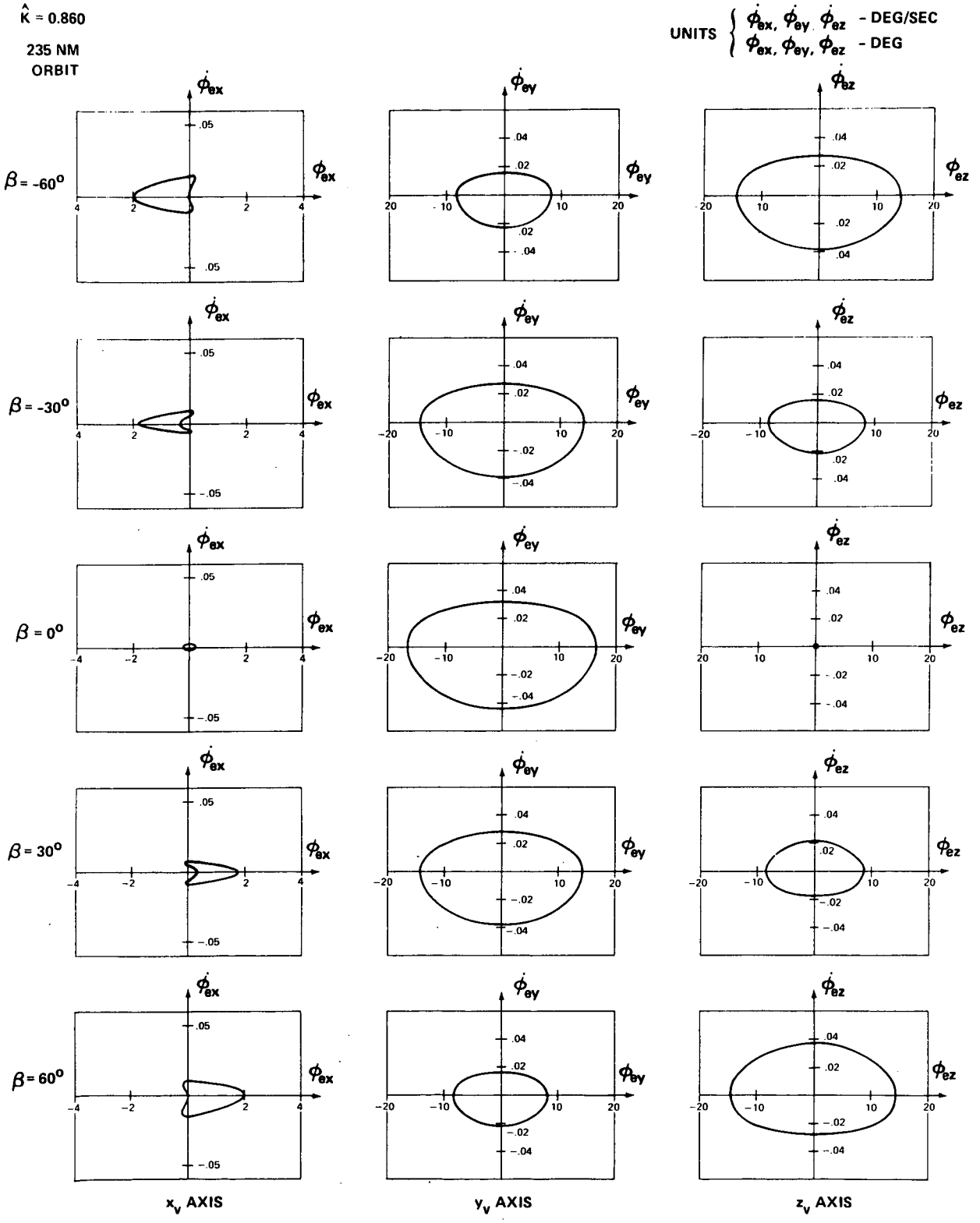

FIGURE 6 - PHASE TRAJECTORIES OF QI MOTION COMPONENTS ON SKYLAB GEOMETRIC AXES (x_v, y_v, z_v)

The larger attitude deviation increases the instantaneous loss in electrical power from the solar arrays. However, the average energy loss per orbit sunlight interval is only 12% at most. Since the minimum of δ_{zv} usually exceeds 2°, little use of the ATM, as discussed earlier for the QI mode, could be expected.

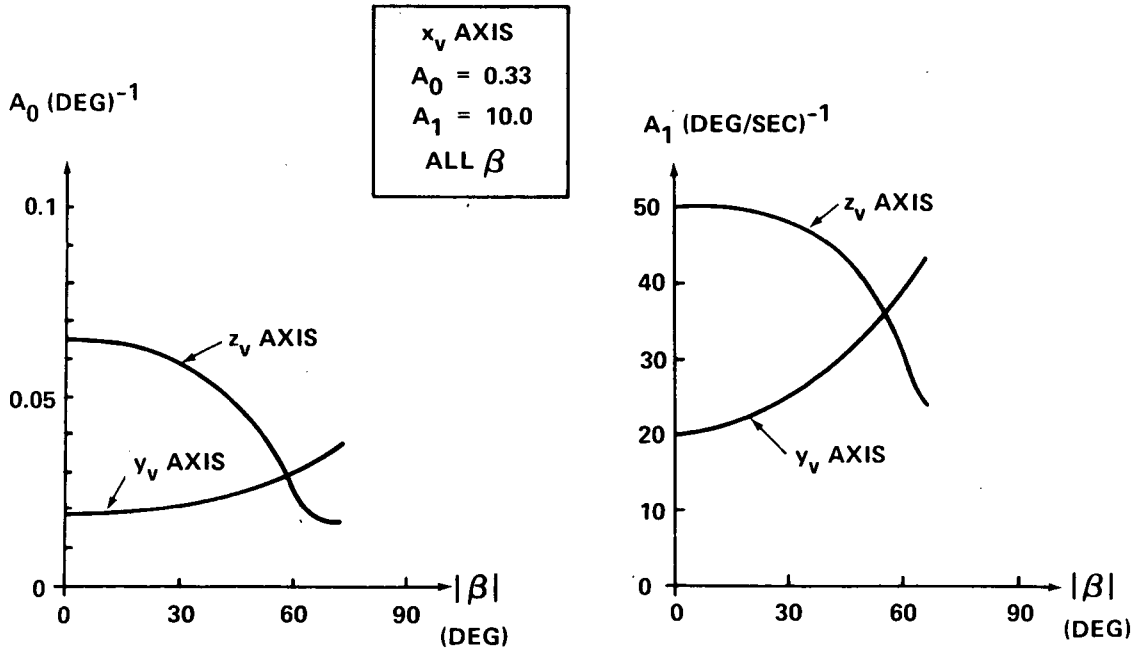

FIGURE 7 - CONTROL LAW PARAMETERS (A_0, A_1) vs β FOR WDB MODE

4.0 Propellant Requirements for Maintaining the Quasi-Inertial and Wide-Deadband Modes

In the two preceding sections spacecraft motion in the QI and WDB modes has been described. In this section propellant requirements for maintaining each mode are presented and compared with that for the solar-inertial (SI) mode. The results are given in terms of total force impulse (lb-sec) per orbit required with either OA/TACS or SM/RCS control.

4.1 Theoretical Impulse Requirement - QI Mode

In Appendix A the theoretical impulse requirement for maintaining the QI mode is evaluated analytically under the following assumptions:

a) only gravity-gradient torque acts on the spacecraft,*

b) the principal and geometric x axes (x_p and x_v) are coincident,

c) the spacecraft center-of-mass (CM) lies along the x_v axis,

d) the effective thruster force directions lie in a plane normal to the x_v axis, and

e) the thruster minimum impulse is sufficiently low that a required control torque profile can be approximated by a sequence of minimum impulse firings.

No restriction is placed on the relative orientation about x_v of transverse (y,z) prinicpal, geometric and thruster control axes as indicated in Figure 8.**

The total force impulse (I_T) required per orbit can be stated as

$$I_T = \frac{1}{r_x} \int_0^T |T_{cx}^t| dt + \frac{1}{r_{yz}} \left[\int_0^T |T_{cy}^t| dt + \int_0^T |T_{cz}^t| dt \right] \qquad (16)$$

---

*For the Skylab mission and nominal mission parameters (235 NM circular orbit and November, 1972 launch date) aerodynamic torque is relatively small compared to gravity-gradient torque.

**CSM clocking relative to the OA geometric axes shifts the the SM/RCS transverse control axes (y_c, z_c) by ϕ_c.[5] Note the definition of $\hat{\phi}$ in Figure 8 and typical values for OA/TACS and SM/RCS control in the accompanying table.

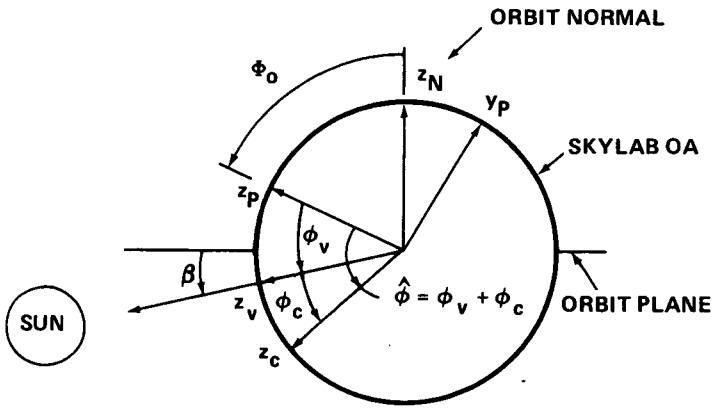

SKYLAB PARAMETERS†

	ϕ_v	ϕ_c	$\hat{\phi}$
OA/TACS	16.6°	0°	16.6°
SM/RCS	16.6°	−27.75°	−11.15°

† Data Based on Refs. (4) and (5)

FIGURE 8 - RELATIVE ORIENTATION OF PRINCIPAL, GEOMETRIC AND THRUSTER CONTROL AXES

where $(T_{cx}^t, T_{cy}^t, T_{cz}^t)$ are components of the required control torque resolved along TACS or RCS control axes, r_x and r_{yz} are effective thruster lever arms relative to the spacecraft CM and T is the orbital period. Evaluation of I_T described in Eqs. (A-34) - (A-51) leads to a relationship involving spacecraft inertia parameters $(K_y, K_z, \hat{k})$* and four other parameters: $\hat{K}$, Φ_o, $\hat{\phi}$ and $\hat{r} \equiv r_x/r_{yz}$. The result is**

$$I_T = I_{mx}[F(\hat{K})|\sin 2\Phi_o| + \hat{r}G(\hat{K})H(\hat{K}, \Phi_o, \hat{\phi})] \qquad (17)$$

where F, G and H are defined in Eqs. (A-51), (A-52) and (A-46). Also see Figure (A-7). The first term in Eq. (17) is related to the x axis component of the impulse requirement and the second to the y and z axis components.

---

*See Appendix C for the definition of K_y, K_z and $\hat{k}$.

**The term, I_{mx}, a constant for any given orbit and spacecraft configuration, represents the impulse per orbit required to overcome the bias component of x axis gravity-gradient torque at $\Phi_o = \pm 45°$ or $\pm 135°$. See Eqs. (A-55) and (A-10).

Generally $\hat{\phi}$ and $\hat{r}$ are fixed by the spacecraft configuration and Φ_o by the spacecraft pointing requirements. However, $\hat{K}$ may be selected so as to minimize I_T. Representative plots of I_T vs $\hat{K}$ are shown in Figure 9 for $|\Phi_o|=45°$ and Skylab parameters $(\hat{\phi},\hat{r},I_{mx})$ listed in the accompanying table. Note that $\hat{K}=0$ corresponds to the SI mode so that better than an order

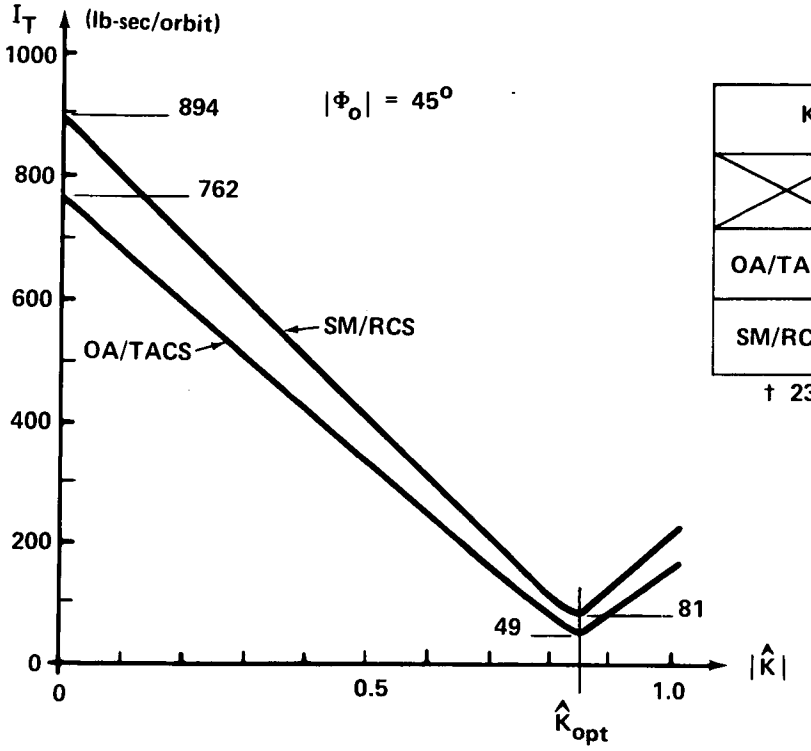

SKYLAB PARAMETERS

$K_y = 0.834$, $K_z = 0.860$, $\hat{k} = -0.014$			
	$\hat{\phi}$	$\hat{r}$	I_{mx} †
OA/TACS	16.6^o	0.24	29.5 lb-sec
SM/RCS	-11.15^o	0.16	50.0 lb-sec

† 235 NM Circular Orbit

FIGURE 9 - THEORETICAL IMPULSE REQUIREMENT IN THE QI MODE vs $\hat{K}$

of magnitude reduction in impulse requirements is attainable by appropriate choice of $\hat{K}$. In Appendix A an optimal choice $(\hat{K}_{opt})$ has been derived as a function of inertia parameters $(K_y,K_z,\hat{k})$ and rotation parameters $(\Phi_o,\hat{\phi})$.

Curves of I_T vs $|\Phi_o|$ corresponding to $\hat{K} = \hat{K}_{opt}$, K_y and K_z are shown in Figure 10 for OA/TACS control. Similar curves result for SM/RCS control with a peak impulse requirement near 80 lb-sec/orbit. It is clear that $\hat{K}_{opt} = K_y$ for $|\Phi_o|=90°$

and $\hat{K}_{opt} = K_z$ for $\Phi_o = 0°, 180°$. Each of these cases corresponds to conditions where the QI mode is a natural motion with zero control impulse requirement. It can be shown that $\hat{K}_{opt}$ always lies within the interval or very close to the end points of the interval bounded by K_y and K_z for all Φ_o and $\hat{\phi}$. In fact a useful approximation for $\hat{K}_{opt}$ with negligble increase in I_T over the optimal is given by

$$\hat{K} = K_z \cos^2\Phi_o + K_y \sin^2\Phi_o \simeq \hat{K}_{opt} \qquad (18)$$

Thus for the Skylab configuration $\hat{K}_{opt}$ ranges typically between $K_y = 0.83$ and $K_z = 0.86$. In view of Figure 2 the corresponding oscillation amplitude ($\Delta\Psi_m$) in the QI mode ranges between 16.2° and 16.6°. Of course, as a practical matter, $\hat{K}$ may simply be fixed at the lower limit (K_y) for all Φ_o and the slight increase in impulse requirements traded off for simplicity in software design.

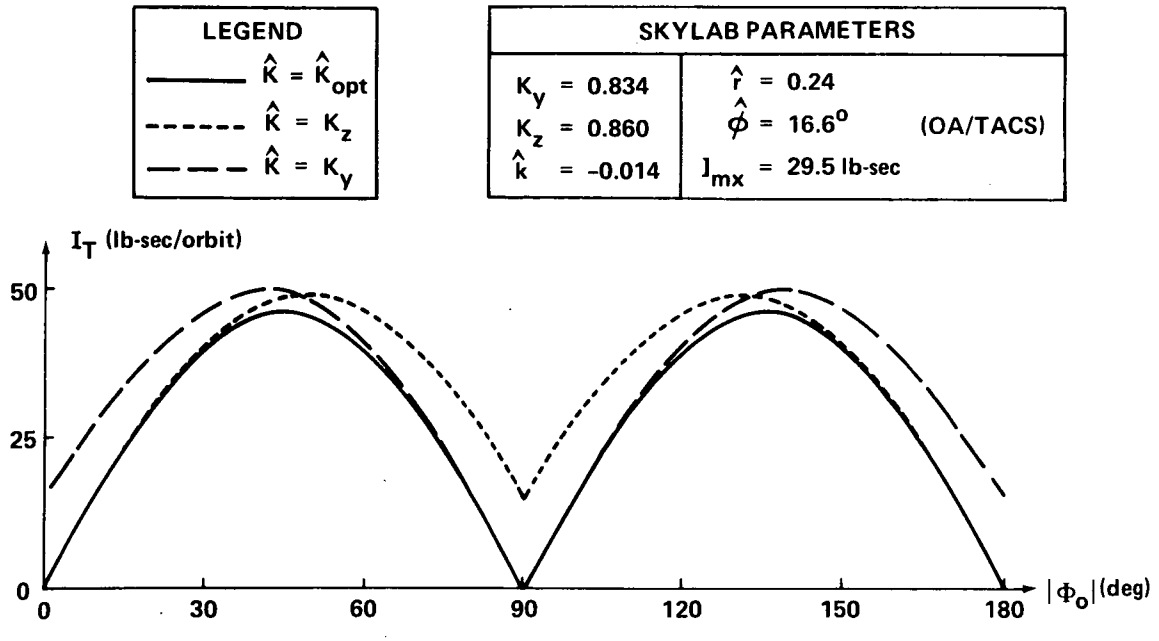

FIGURE 10 - THEORETICAL IMPULSE REQUIREMENT FOR THE QI MODE vs Φ_o (WITH OA/TACS CONTROL)

As noted earlier Φ_o is determined by the roll axis pointing requirement, which is usually stated in terms of β. An approximate relationship between Φ_o and β based on Figure 8 (x_p and x_v assumed parallel) is given by*

$$\Phi_o \simeq (90° + \beta) - \phi_v = 73.4° + \beta \qquad (19)$$

Since β ranges between $\pm 73.5°$ for a 50° orbit, the maximum impulse requirement corresponding to $\Phi_o = 45°$ and 135° will occur at $\beta = -28.4°$ and $+61.6°$.

4.2 Simulation Results - QI, WDB and SI Modes

Analytical evaluation of impulse requirements for reaction thrust systems is usually feasible only if the spacecraft motion is known and certain simplifying assumptions on the spacecraft configuration and disturbance environment are imposed. That approach was useful for the QI mode in arriving at an optimal parameter selection ($\hat{K}_{opt}$). To confirm these results and to determine the impulse requirements for the WDB and SI modes including the effect of aerodynamic torque, a computer simulation of the Skylab OA configuration[4,5,12] was utilized.

The results for OA/TACS control are shown in Figure 11 as a function of β. (Note the scale change on the ordinate axis) The data for the WDB mode** are based on selecting control law parameters A_0 and A_1 (per control axis) as a function of β according to Figure 5. Results for the QI mode are based on $\pm 0.5°$

---

*An exact relationship between Φ_o and β is given in Appendix A.3, Eq.(A-32). See Figure (A-5).

**The impulse requirements for the WDB mode are not claimed to be the optimal, although they represent a significant reduction compared to those for the SI mode. It also must be noted however, that the impulse data are based on long time averages (10 orbits). Transient conditions resulting from venting torques will tend to increase the impulse requirement since they force the spacecraft out of the low-impulse limit cycle motion, which then must be reacquired. This increase is over and above the requirement to remove the disturbance impulse, if tight attitude control was maintained, as in the SI and QI modes.

deadbands and $\hat{K} = \hat{K}_{opt}$ as approximated by Eqs. (18) and (19). Aerodynamic torque and misalignment ($\sim 4°$)[4] of x_v and x_p axes account for the slight increase in impulse compared to the theoretical results in Figure 10.* Impulse requirements for the SI mode are better than an order of magnitude higher than for the QI mode, as predicted earlier in Section 4.1.

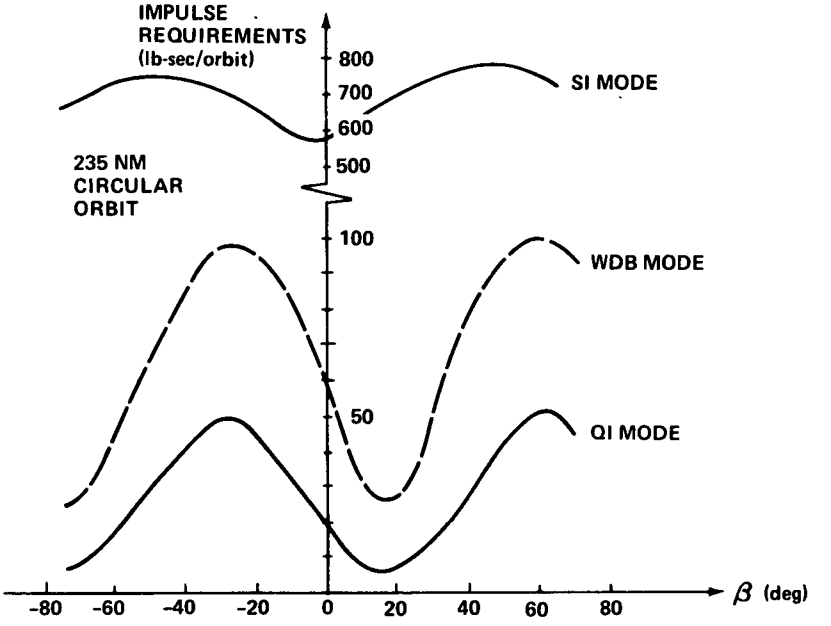

FIGURE 11 - IMPULSE REQUIREMENTS vs β FOR THE QI, WDB AND SI MODES WITH OA/TACS CONTROL

Similar results are obtained with SM/RCS control of the Skylab. The corresponding peak impulse requirements are 85, 164 and 898 lb-sec/orbit for the QI, WDB and SI modes respectively. Selection of control law parameters A_0 and A_1 for the WDB mode with SM/RCS control must be modified slightly. Since these parameters are based on the component of the QI motion appearing on a given control axis, it is necessary to shift the abscissa scale in Figure 5 to account for the CSM clocking relative to the OA/TACS control axes (x_v, y_v, z_v). In view of Figure 8 the necessary shift is given by ϕ_c. Hence for a given β, control law parameters, A_0 and A_1, should be selected from Figure 5 on the basis of $\beta_c \equiv \beta + \phi_c$.

---

*The WDB mode can be interpreted as a "sloppy" QI mode, since no command rate is used. Hence, it is reasonable to anticipate that small errors in initialization $(\psi_o, \dot{\psi}_o)$ and non-optimal $\hat{K}$ (but $\hat{K}$ near $\hat{K}_{opt}$) would result in an actual QI mode impulse requirement somewhere between the QI and WDB mode curves in Figure 11.

The impulse requirements with SM/RCS control can also be estimated from the results for OA/TACS control by considering the expression for impulse I_T in Eq. (16) written as

$$I_T = \frac{1}{r_x} [J_x + \hat{r}\, J_{yz}] \tag{20}$$

where

$$J_x \equiv \int_0^T |T_{cx}| dt \tag{21}$$

$$J_{yz} \equiv \int_0^T |T_{cy}| dt + \int_0^T |T_{cz}| dt \tag{22}$$

and $\hat{r} \equiv r_x/r_{yz}$ as before. For any given mode and nominal spacecraft roll orientation (β), control torque impulses J_x and J_{yz} are fixed by the disturbance environment. The parameters r_x and $\hat{r}$ however, depend on the controller (OA/TACS or SM/RCS). See Table I for typical values:

TABLE I

EFFECTIVE THRUSTER LEVER ARMS FOR SKYLAB OA†

CONTROLLER \ PARAMETER	r_x	r_{yz}	$\hat{r} = r_x/r_{yz}$
OA/TACS	130″	552″	0.24
SM/RCS	77″	490″	0.16

† Based on Data from References (4) and (5)

Hence, the ratio (ρ) of impulse requirements for SM/RCS and OA/TACS control can be expressed as

$$\rho \equiv \frac{I_{T\ RCS}}{I_{T\ TACS}} = \frac{r_{x\ TACS}}{r_{x\ RCS}} \left[\frac{J_x + \hat{r}_{RCS}\ J_{yz}}{J_x + \hat{r}_{TACS}\ J_{yz}} \right]$$

$$= 1.7 \left[\frac{J_x + 0.16\ J_{yz}}{J_x + 0.24\ J_{yz}} \right] \tag{23}$$

In the SI mode $\hat{r}\, J_{yz} >> J_x$ so that $\rho \simeq 1.13$. But in the QI mode and approximately so in the WDB mode, $\hat{r}\, J_{yz} << (J_x)_{max}$* so that $\rho_{max} \simeq 1.7$. Thus, impulse requirements for SM/RCS control generally exceed those for OA/TACS control as should be expected because of the smaller effective lever arms. These observations are consistent with simulation results and the prior theoretical analysis. (See Figure 9 for $\hat{K} = 0$ and $\hat{K} = \hat{K}_{opt}$)

4.3 Mission Duration in the QI, WDB and SI Modes with OA/TACS or SM/RCS Control

Extension of the Skylab mission with the OA/TACS or SM/RCS in the event of two CMG failures will depend on the propellant balance and the attitude control mode utilized. A conservative estimate of this extension is given below for the QI, WDB and SI modes. The data are based on peak impulse requirements for each mode, and operation only with currently projected propellant impulse margins, as listed in Table II.**

TABLE II

PROPELLANT MARGINS AND PEAK IMPULSE REQUIREMENTS

	PROPELLANT IMPULSE MARGINS (6) (lb-sec)	PEAK IMPULSE REQUIREMENTS† (lb-sec/orbit)		
		QI MODE	WDB MODE	SI MODE
OA/TACS	35,860	52	98	780
SM/RCS	42,400 (± 5,300)	85	164	898

† 235 NM circular orbit

---

*$(J_x)_{max}$ corresponds to $|\Phi_o| = 45°$ or $135°$ where $|s2\Phi_o| = 1$.

**The TACS margin is the value at the end of the SL-4 mission (third CSM). The SM/RCS propellant weight margin is listed in Reference (6) as 319.8 lbs. Only 268.0 lbs. is actually available however, since the balance is reserved for de-orbit back-up. The ±5300 lb-sec tolerance on impulse margins in Table II corresponds to the bounds on SM/RCS specific impulse (I_{sp}) for minimum impulse thruster firings. (min I_{sp}=135, max I_{sp}=178, nominal I_{sp}=157) (5) No tolerance on the OA/TACS impulse margin is shown, since the thruster minimum impulse bit is maintained at 4.0 lb-sec. (1)

The extension in mission duration can be estimated in each case from

$$\text{Mission Duration (days)} = \frac{\text{Propellant Impulse Margin}}{\text{Impulse Requirement} \times 15.4} \qquad (24)$$

where 15.4 is the number of orbits per day in the 235 x 235 NM Skylab orbit. The results are tabulated in Table III. The variation in mission duration figures for SM/RCS control is due to the possible range on thruster specific impulse.

TABLE III

MISSION DURATION (DAYS) WITH OA/TACS OR SM/RCS CONTROL

MODE / CONTROLLER	QI	WDB	SI
OA/TACS	45	24	3
SM/RCS	33 (±4)	17 (±2)	3 (±0.4)

These results show that a full 28 day mission could be achieved in the QI mode with either OA/TACS or SM/RCS control. A full 56 day mission is obtainable with both OA/TACS and SM/RCS control (in sequence). Since the figures for SM/RCS control are based on conservative propellant margins,* it is conceivable (at least from impulse considerations), that a 56 day mission could be achieved without the OA/TACS contribution. This would permit completion of the full Skylab mission (SL-1,2,3,4), if two CMG failures occurred as early as the beginning of the SL-1/SL-3 segment. See Figure 12.

---

*The SM/RCS propellant weight budget for SL-2[6] lists 400 lbs for rendezvous dispersions and alleviations for mission flexibility (e.g. stationkeeping, workshop fly-around) compared to the 268 lb margin used in this analysis. Availability of 185 lbs from this or other sources would increase the 33 day duration figure in Table III to 56 days.

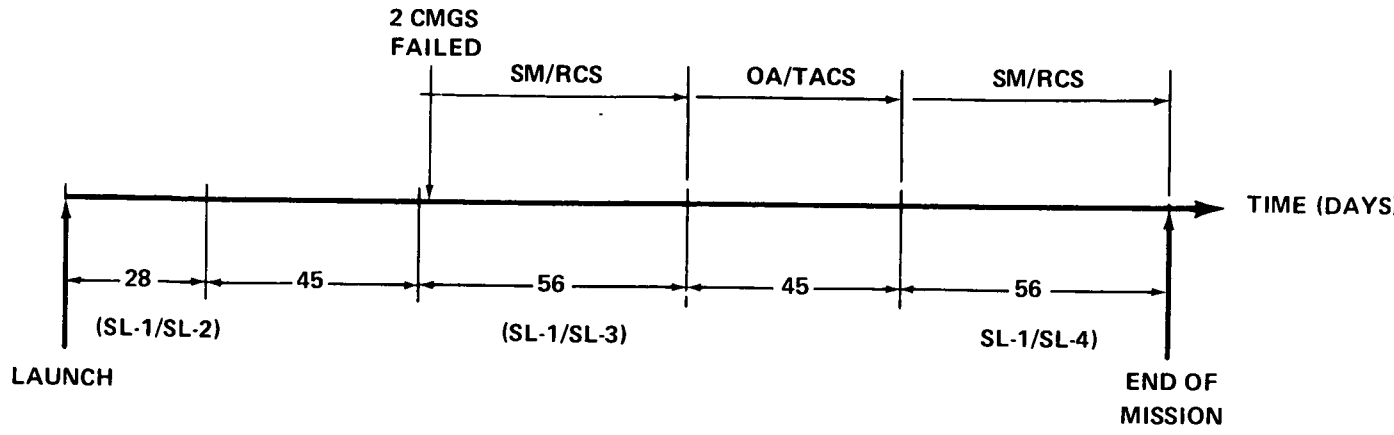

FIGURE 12 - POSSIBLE SKYLAB MISSION SEGMENTS WITH OA/TACS AND SM/RCS CONTROL IN QI MODE

Extension of the mission duration with the WDB mode is also considerable compared with the SI mode. One 28 day mission could be easily achieved with OA/TACS and SM/RCS control (in sequence). Extension of the mission for one more CSM visit would not be likely if two CMGs failed earlier than 24 days before the next CSM launch (SL-3 or SL-4).

5.0 Attitude Update Requirements for the QI and WDB Modes

Requirements for attitude updating are influenced by several factors. First, the OA/TACS "strapdown" reference and the CSM inertial platform reference (IMU) must be updated to compensate for component error sources, primarily gyro drift rates. Second, navigational computations defining the solar inertial orientation, which is the desired nominal attitude in the QI and WDB modes, must be updated to account for the earth's annual rotation about the sun and orbital regression effects.* Finally, in the QI mode, the parameter ψ_o used in command rate computations should be updated to account for cumulative integration errors and slow changes in the solar vector orientation and vehicle inertia properties over the mission.

---

*This capability already exists in the ATMDC for OA/TACS control but not in the CMC for SM/RCS control.

5.1 Attitude Reference Updates

Sensors available for attitude reference updating include the acquisition sun sensor and star tracker for the OA/TACS strapdown reference and optical telescope and sextant for the CSM IMU. Drift rate specifications for the strapdown reference and IMU gyro/electronic amplifier packages are 0.1°/hr and 0.03°/hr respectively.[5] Hence a 1° tolerance in the attitude reference implies an update requirement of about once every 6 orbits for the strapdown reference and once every 20 orbits for the IMU. The IMU alignment requires astronaut participation, but the strapdown reference update could be done automatically.

Time variation of the solar pointing error in the QI and WDB modes is shown in Figure 13 for β=16°.* Typically, the pointing error falls within the linear range of the acquisition sun sensor ($\pm$6°) four times per orbit so that at least three opportunities occur each orbit for a two-axis update of the strapdown reference.** Star tracker gimbal angles provide data for the third axis update.

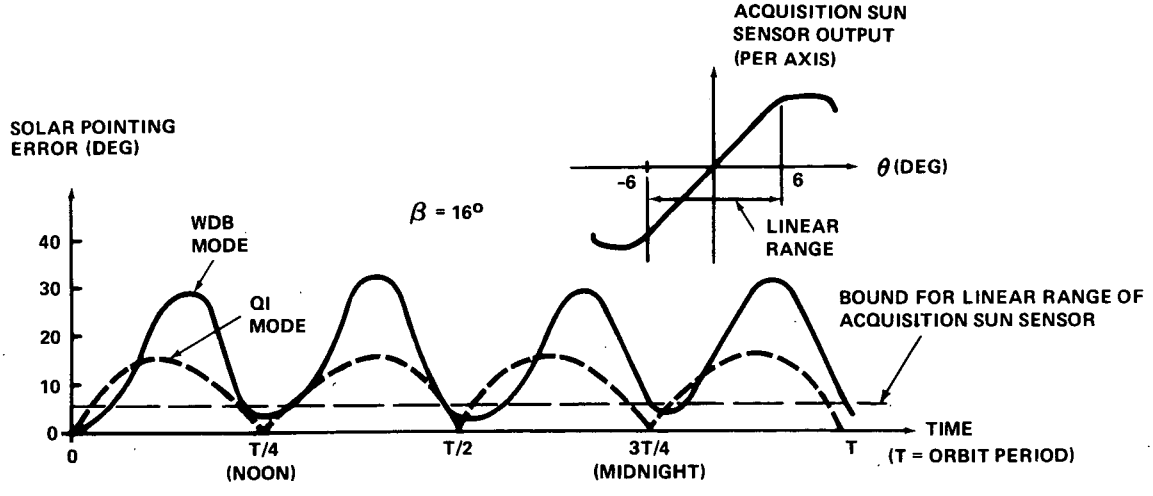

FIGURE 13 - TYPICAL VARIATION OF SOLAR POINTING ERROR IN QI AND WDB MODES

*The pointing error for the QI mode is expressed analytically by δ_{zv} in Eq. (14). The maximum error in any orbit decreases with increasing $|\beta|$. Characteristically however, the maximum pointing error in the WDB mode does not decrease with β.

**A fourth opportunity occurs near orbital midnight in all-daylight orbits. The total orbit interval during which the pointing error lies within 6° is plotted in Figure 3 as a function of β for the QI mode. The interval is less for the WDB mode.

5.2 Solar Inertial Update

ATMDC software provides for computing parameters specifying the solar inertial orientation relative to the orbital plane.[1] A similar capability would be needed in the CMC for SM/RCS control.

In the QI mode the computational results are needed to transform the desired command rate ($\dot{\underline{\Theta}}_C$) into appropriate coordinates: (x_V, y_V, z_V) for OA/TACS control and (x_C, y_C, z_C) for SM/RCS control.* Continuous updating, which accounts for the change in the solar inertial orientation, can be achieved by a composite command rate ($\dot{\underline{\Omega}}_C$), that combines the regression rate ($\dot{\underline{\lambda}}$) and annual rate ($\dot{\underline{\Gamma}}$) with $\dot{\underline{\Theta}}_C$ so that**

$$\dot{\underline{\Omega}}_C = A\,\dot{\underline{\Theta}}_C + B\,\dot{\underline{\lambda}} + C\,\dot{\underline{\Gamma}} \qquad (25)$$

where $\dot{\underline{\Theta}}_C$ is given by Eq. (13) and A, B and C are appropriate coordinate transformation.

5.3 QI Mode Updates

The calculation for command rate ($\dot{\underline{\Psi}}$) in Eq. (6) utilizes the QI motion parameter ψ obtained by integrating Eq. (12) with the initial condition ψ_o. If the motion were initiated at orbital noon (η=0), then ψ_o ($=\psi_n$) can be obtained by solving Eq. (9) for a desired nominal orientation Ψ_N, which is related to β and spacecraft inertia characteristics by Eqs. (A-33) and (A-34) in Appendix A. Other points in orbit for initializing ψ would be more convenient, however, in terms of simplifying the required computational algorithm. Natural transition points in the motion ($\Delta\Psi$=0 and $\Delta\Psi=\pm\Delta\Psi_m$) are advantageous, since ψ and the corresponding orbital position (η) are conveniently evaluated.

---

*See Footnote **, p. 15.

**This is discussed in detail in Reference 11.

In general η and ψ are related through Eqs. (3) and (4) by

$$\eta = \Psi_N - \frac{k}{\lambda} F(k,\psi) = (\frac{\pi}{2} + \eta_{tm}) - \frac{k}{\lambda} F(k,\psi) \tag{26}$$

where Eq. (A-33) has been substituted for Ψ_N.* In view of Figure 2 attitude zero crossings ($\Delta\Psi=0$) occur whenever

$$\psi = (3-p)\pi/2 \qquad p = 1, 2, 3, 4 \tag{27}$$

This corresponds to the four points in orbit

$$\eta_p = (\frac{\pi}{2} + \eta_{tm}) - \frac{k}{\lambda} F[k,(3-p)\pi/2]$$

$$= (\frac{\pi}{2} + \eta_{tm}) - (3-p)\pi/2$$

$$= \eta_{tm} + (p-2)\pi/2 \qquad p = 1, 2, 3, 4 \tag{28}$$

where the OA geometric axis z_v points directly to the sun. See Figure 14a. In view of Figure 2 and Eqs. (10) and (11) attitude extremes ($\Delta\Psi=\pm\Delta\Psi_m$) occur whenever

$$\psi = \begin{cases} -\psi_m & \Delta\Psi=-\Delta\Psi_m \quad (r=4) \\ \psi_m & \Delta\Psi=\Delta\Psi_m \quad (r=3) \\ \pi-\psi_m & \Delta\Psi=-\Delta\Psi_m \quad (r=2) \\ -(\pi-\psi_m) & \Delta\Psi=\Delta\Psi_m \quad (r=1) \end{cases} \tag{29}$$

*Physically, η_{tm} represents the nominal orbit angle offset of x_p from an orientation normal to the sunline due to the displacement of principal and geometric x axes (x_p and x_v).

The corresponding four points in orbit are

$$\eta_r = \begin{cases} -\pi/2 + \eta_{tm} + (2r-3)\ k/\lambda\ F(k,\psi_m) & r = 1,2 \\ \pi/2 + \eta_{tm} + (2r-7)\ k/\lambda\ F(k,\psi_m) & r = 3,4 \end{cases} \tag{30}$$

See Figure 14b. These results specify 8 points in orbit for initializing ψ, that is, by Eqs. (27) or (29), whichever is appropriate.

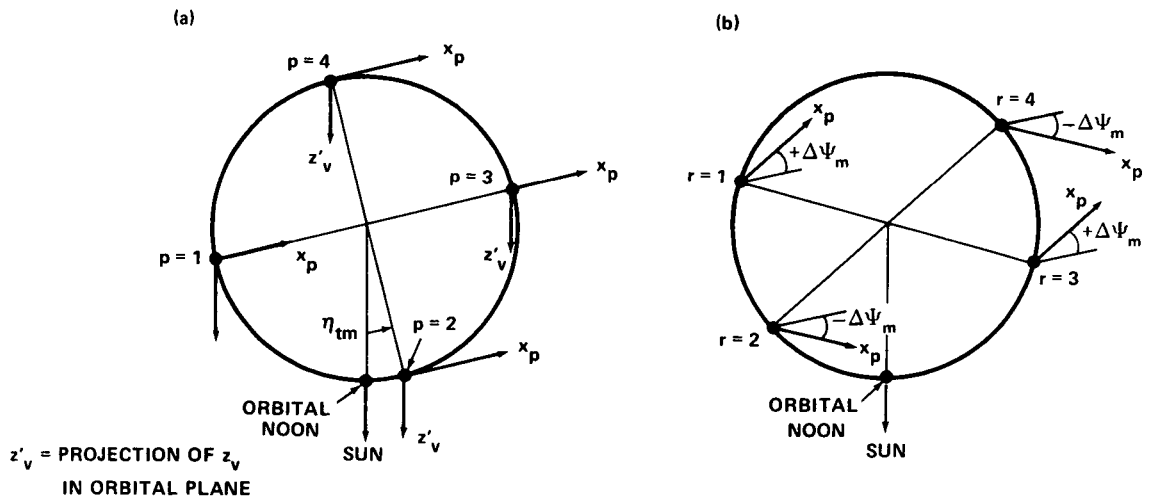

FIGURE 14 - LOCATION IN ORBIT FOR x_p AT NOMINAL AND OSCILLATION AMPLITUDE ORIENTATIONS

Somewhat more flexibility in update time with a simple algorithm for ψ in terms of orbital position (η) can be achieved in the region where $\eta=\eta_p$ (p=1,3) shown in Figure 14a. In this vicinity let

$$\psi = (3-p)\ \pi/2 + \xi \qquad p=1,3 \tag{31}$$

where ξ is a small angle to be determined.

Substitution into Eq. (28) yields*

$$\eta = \eta_{tm} + \pi/2 - (k/\lambda)F[k,(3-p)\pi/2 + \xi]$$

$$= \eta_{tm} + \pi/2 - (3-p)\pi/2 - (k/\lambda)F(k,\xi) \qquad (32)$$

$$= \eta_p - (k/\lambda)F(k,\xi) \qquad (p = 1,3)$$

For $|\xi|<30°$, then $F(k,\xi) \approx \xi$ with negligible error.[3] Hence,

$$\xi \approx -(\lambda/k)(\eta-\eta_p) \qquad (p = 1,3) \qquad (33)$$

The orbit interval about η_p such that $|\xi|<\pi/6$ is $2(k/\lambda)(\pi/6)$ or about 36°.** Hence, two 36° sectors centered at $\eta=\eta_1$ and $\eta=\eta_3$ are available for initializing ψ wherein ψ is related linearly to orbit position by

$$\psi = (3-p)\pi/2 - \lambda/k(\eta-\eta_p) \qquad p = 1,3 \qquad (34)$$

Finally it should be noted that the QI oscillation ($\Delta\Psi$) can be approximated by

$$\Delta\Psi \approx -\Delta\Psi_m \sin 2(\eta-\Psi_N) \qquad (35)$$

---

*A property of elliptic integrals is that $F(k,N\pi+\xi) = 2N\,K(k) + F(k,\xi)$ for N an integer. Here $N = (3-p)/2$, $p = 1,3$. The second step in Eq. (32) follows from Eq. (8).

**A typical value of the ratio λ/k for the Skylab configuration is $\lambda/k = 1.67$.

with at most 1.3° error for any η. Hence from Eqs. (3) and (5) it follows that

$$\psi = \Psi - \eta = \Delta\Psi - (\eta - \Psi_N)$$

$$\simeq -\Delta\Psi_m \sin 2(\eta - \Psi_N) - (\eta - \Psi_N)$$

$$= \pi/2 - [-\Delta\Psi_m \sin 2(\eta - \eta_{tm}) + (\eta - \eta_{tm})] \qquad (36)$$

This provides another expression, although approximate, for initializing ψ for arbitrary η. The result is exact for $\eta = \eta_p$, (p = 1,2,3,4).

6.0 Summary and Conclusions

The Quasi-Inertial (QI) and Wide-Deadband (WDB) modes have been evaluated as possible backup attitude options in the event that two CMGs fail during the Skylab mission. In the QI mode a command rate is utilized with tight limit cycle control such that the x principal axis oscillates in the orbital plane with the solar panels pointed nominally to the sun. In the WDB mode a somewhat similar motion is encouraged without a command rate by appropriate choice of controller deadbands and switch line slopes. Various performance characteristics and operational requirements for each mode are summarized in Table IV for comparison with the Solar Inertial (SI) mode.

Both the QI and WDB modes provide substantial reductions in propellant requirements that are reflected in the significant increase in potential mission duration over the SI mode. With SM/RCS control in the QI mode during CSM visits and OA/TACS control during the storage period (45 days max) it is conceivable that both SL-3 and SL-4 segments of the Skylab mission could be completed, if 2 CMGs fail as early as the SL-3 launch.

Performancewise, the QI mode is superior to the WDB mode, but this option requires software modifications. Nevertheless, software modifications can be uplinked to the ATMDC for OA/TACS control and a subroutine addition to the CMC program is probably preferable to a CSM/DAP modification for SM/RCS control. Finally it should be noted that the WDB mode is not insensitive to venting disturbances that can force the spacecraft out of the low impulse limit cycle motion, which then must be reacquired. (See Footnote**, p. 19)

TABLE IV

SUMMARY OF PERFORMANCE CHARACTERISTICS AND SIGNIFICANT OPERATIONAL REQUIREMENTS FOR THE QI, WDB AND SI MODES WITH THE OA/TACS OR SM/RCS

			QI MODE	WDB MODE	SI MODE
PERFORMANCE CHARACTERISTICS	MAXIMUM SOLAR POINTING ERROR (DEG)		5-17*	35	0.5
	ELECTRICAL ENERGY OUTPUT PER ORBIT FROM SOLAR ARRAYS (% OF SI MODE)		99.5-99.9*	88-90*	100
	SOLAR VISIBILITY INTERVAL WITH ATM (% OF ORBIT)		6-28*	NEGLIGIBLE	61-100*
	POTENTIAL MISSION DURATION**	OA/TACS	45	24	3
		SM/RCS	33 (56 LIKELY)††	17 (28 LIKELY)††	3 (4 LIKELY)††
OPERATIONAL REQUIREMENTS	PROPELLANT IMPULSE PER ORBIT† (% OF SI REQUIREMENT)	OA/TACS	2-7*	5-15*	100
		SM/RCS	3-8*	8-18*	100
	SOFTWARE IMPACT (CONTROL FUNCTION)	OA/TACS (ATMDC)	SUBROUTINE TO GENERATE COMMAND RATE (SEE APPENDIX D)	CHANGE IN CONTROL LAW PARAMETERS (DEADBAND & SWITCH-LINE SLOPE)WITH β MUST BE UPLINKED OR STORED IN ATMDC	NONE
		SM/RCS (CMC)	SUBROUTINE TO GENERATE COMMAND RATE (SEE APPENDIX D)	CSM/DAP MODIFICATION TO PERMIT INDEPENDENT SELECTION OF DEADBAND & SWITCH-LINE SLOPE PARAMETERS FOR EACH CONTROL AXIS WHICH CHANGE WITH β	NONE
	SOFTWARE IMPACT (ATTITUDE REFERENCE UPDATE)	OA/TACS (ATMDC)	SUBROUTINE TO UPDATE STRAPDOWN REFERENCE FROM ACQUISITION SUN SENSOR DATA AND STAR TRACKER GIMBAL ANGLES		
		SM/RCS (CMC)	SUBROUTINE TO GENERATE COORDINATE TRANSFORMATIONS BETWEEN SOLAR INERTIAL AND INERTIAL (IMU) REFERENCE		

* DEPENDS ON β (ANGLE BETWEEN SUN LINE AND ORBITAL PLANE).

** BASED ON MAXIMUM IMPULSE REQUIREMENT FOR ALL β AND CURRENTLY PROJECTED IMPULSE MARGINS (SEE SECTION 4.3 AND TABLE III).

† BASED ON IMPULSE PER ORBIT FOR CONTROL AGAINST GRAVITY GRADIENT AND AERODYNAMIC DISTURBANCE TORQUES. (OTHER NOMINAL USAGE IS NOT INCLUDED, e.g. REQUIREMENTS FOR RENDEZVOUS, DOCKING AND VENTING).

†† SEE SECTION 4.3 AND FOOTNOTE *, p. 19.

Acknowledgement

Recognition is due to W. H. Hamby of NASA Headquarters for suggesting the possible application of previous work on the Quasi-Inertial[2] and Wide-Deadband[7] ideas to the Skylab mission.

B. D. Elrod

1022-BDE-mef
cds

Attachments

APPENDIX A

Quasi-Inertial Orientation of Orbiting Spacecraft

A motion wherein an orbiting spacecraft oscillates about the normal to the orbital plane with one principal axis in the orbital plane is defined as the Quasi-Inertial (QI) mode. The purpose of this Appendix is to develop the conditions for establishing the QI mode, examine the impact on inertial pointing capability and to determine the optimal choice of parameters for minimizing the propellant requirements for maintaining the mode. While this subject has been treated before[2], the present approach takes a more general viewpoint and includes some new results.

A.1 Spacecraft Motion in the QI Mode

The dynamical equations governing spacecraft rotational motion follow from Newton's second law (expressed in vector/matrix notation in body coordinates)*

$$I\dot{\underline{\omega}} + \tilde{\underline{\omega}}I\underline{\omega} = \underline{T}_d + \underline{T}_c \qquad \text{(A-1)}$$

where

$\underline{\omega}$ = total spacecraft angular velocity

I = spacecraft principal axis inertia tensor

$\underline{T}_d$ = external torque acting on the spacecraft

$\underline{T}_c$ = control torque applied to the spacecraft

---

*Underscored Greek or English letters represent (3×1) vectors and upper case English letters represent (3×3) matrices (when defined). A letter superscript may be used with a vector or its components to emphasize the associated coordinate system. The tilde symbol over $\underline{\omega}$ denotes the matrix equivalent to the cross product operation $(\underline{\omega}x)$.

The kinematical equations for relating the orientation of spacecraft principal axes (x_p, y_p, z_p) to an orbit reference system (x_N, y_N, z_N) are based on the Euler angle sequence (Ψ, θ, Φ) shown in Fig.(A-1). This yields

$$\underline{\omega} = \begin{bmatrix} 1 & 0 & -\sin\theta \\ 0 & \cos\Phi & \cos\theta \sin\Phi \\ 0 & -\sin\Phi & \cos\theta \cos\Phi \end{bmatrix} \begin{pmatrix} \dot{\Phi} \\ \dot{\theta} \\ \dot{\Psi} \end{pmatrix} \equiv D\dot{\underline{\xi}} \qquad \text{(A-2)}$$

or

$$\dot{\underline{\xi}} = D^{-1}\underline{\omega} \qquad \theta \neq \pm\pi/2 \qquad \text{(A-3)}$$

In this analysis the principal axis (x_p) is assumed to lie in the orbital plane and conditions for oscillatory motion of x_p are examined. By direct substitution it can be verified that Eqs.(A-1) and (A-2) are satisfied by the motion*

$$\underline{\omega} = \begin{pmatrix} 0 \\ \dot{\Psi} s\Phi_o \\ \dot{\Psi} c\Phi_o \end{pmatrix} \qquad \text{(A-4)}$$

$$\Phi(t) = \Phi_o \ , \quad \text{a constant} \qquad \text{(A-5)}$$

$$\theta(t) = 0 \qquad \text{(A-6)}$$

$$\ddot{\Psi} = -\frac{3\Omega_o^2}{2} \hat{K} s2(\Psi - \eta) \qquad \text{(A-7)}$$

---

*For brevity the notation $c\alpha$ and $s\alpha$ is used for the trigonometric operations $\cos\alpha$ and $\sin\alpha$, α arbitrary.

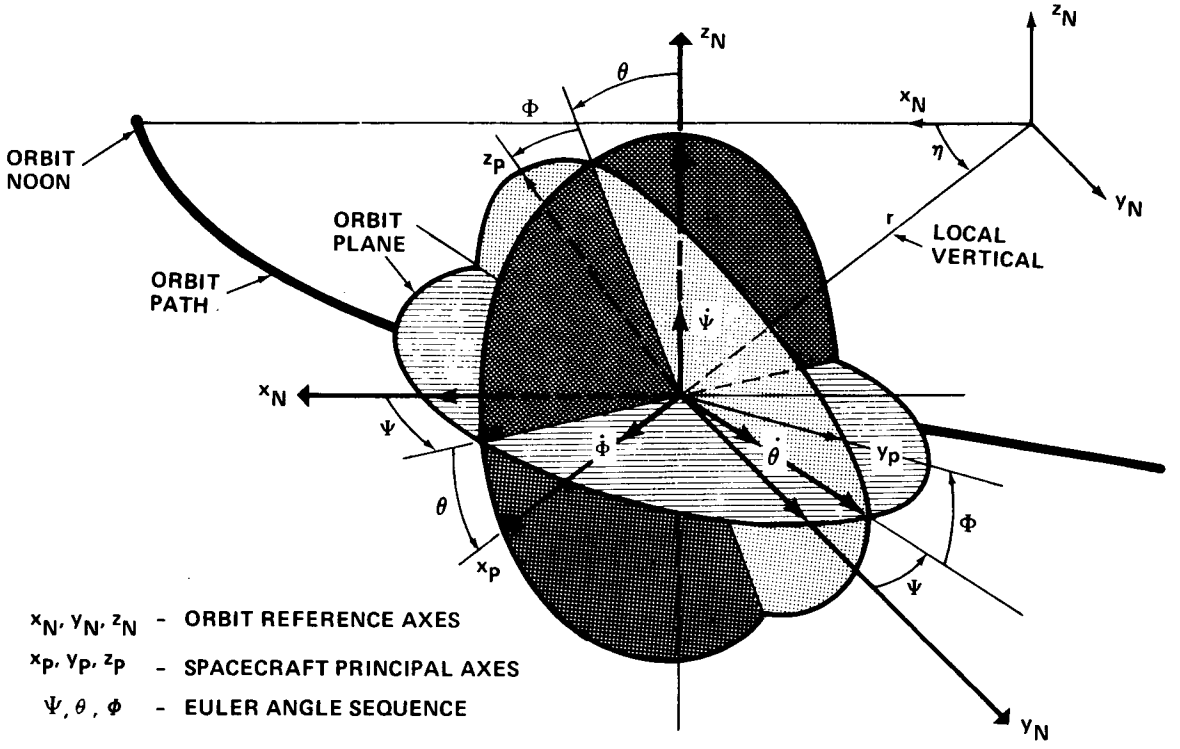

FIGURE A-1a - GENERAL SPACECRAFT ATTITUDE RELATIVE TO ORBIT REFERENCE AXES

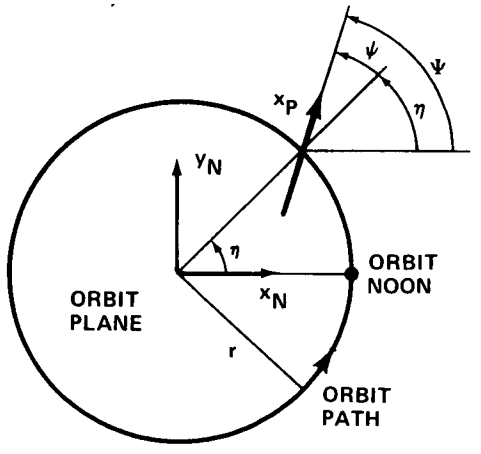

FIGURE A-1b - ORIENTATION OF x_P IN QI MODE

$$\underline{T}g = -3\Omega_0^2/2 \begin{pmatrix} (I_z - I_y)\,A \\ (I_z - I_x)\,B \\ (I_y - I_x)\,C \end{pmatrix}$$

$$\Omega_0^2 = \mu_E / r^3$$

$$A = \sin 2\phi\,[\sin^2(\Psi - \eta) - \sin^2\theta\cos^2(\Psi - \eta)] + \cos 2\phi \sin\theta \sin 2(\Psi - \eta)$$

$$B = \sin\phi\cos\theta \sin 2(\Psi - \eta) + \cos\phi \sin 2\theta \cos^2(\Psi - \eta)$$

$$C = \cos\phi\cos\theta \sin 2(\Psi - \eta) - \sin\phi \sin 2\theta \cos^2(\Psi - \eta)$$

FIGURE A-1c - GRAVITY GRADIENT TORQUE

if $\underline{T}_d = \underline{T}_g^p$ (the gravity-gradient torque defined in Fig.A-1), the orbit is circular, i.e.,*

$$\eta = \Omega_o (t-t_n) \tag{A-8}$$

and the control torque is

$$\underline{T}_c^p = \begin{pmatrix} T_{cx} \\ T_{cy} \\ T_{cz} \end{pmatrix}^p = T_{gmx} \begin{pmatrix} s2\Phi_o [s^2(\Psi-\eta) + \frac{1}{3}(\dot{\Psi}/\Omega_o)^2] \\ s\Phi_o \; s2(\Psi-\eta)(K_y-\hat{K})(1-\hat{k})/\hat{k} \\ c\Phi_o \; s2(\Psi-\eta)(K_z-\hat{K})/\hat{k} \end{pmatrix} \tag{A-9}$$

In Eq. (A-9)

$$T_{gmx} \equiv \frac{3\Omega_o^2}{2}(I_z-I_y) \tag{A-10}$$

represents the maximum x_p axis gravity-gradient torque. The parameters K_y, K_z and $\hat{k}$ are functions of the spacecraft principal axis inertias as defined in Appendix C. The parameter $\hat{K}$ is a constant to be specified. Note that no control torque is required to sustain the motion when a) the spacecraft is symmetrical ($I_z=I_y$) or b) $\Phi_o=0$, 180° and $\hat{K}=K_z$ or c) $\Phi_o=\pm 90°$ and $\hat{K}=K_y$. The latter two cases correspond to two principal axes lying in the orbital plane.

Motion of the x_p axis can be interpreted in terms of the variable

$$\psi \equiv \Psi - \eta = \Psi - \Omega_o (t-t_n) \tag{A-11}$$

---

*Here η is orbit position relative to orbital noon, Ω_o is orbit angular velocity, t is absolute time and t_n is absolute time at last orbital noon.

which is the deviation of x_p from the local vertical. (See Fig. A-1.) In view of Eqs. (A-7) and (A-11), the differential equation for ψ is

$$\ddot{\psi} = -\frac{3\Omega_o^2}{2}\hat{K}s2\psi = -Bs2\psi \qquad \text{(A-12)}$$

which is analogous to the differential equation for a simple pendulum. As with the pendulum two possible solutions exist: periodic and continuous revolution. For the motion $\Psi(t)$ to be periodic however, it follows that

$$\dot{\Psi}_{ave} = (\dot{\psi}+\dot{\eta})_{ave} = \dot{\psi}_{ave} + \Omega_o = 0 \qquad \text{(A-13)}$$

or

$$\dot{\psi}_{ave} = -\Omega_o < 0 \qquad \text{(A-14)}$$

which corresponds to continuous revolution of x_p about the local vertical, once per orbit. Integrating Eq. (A-12) twice yields

$$\dot{\psi}(t) = -\frac{\lambda}{k}\Omega_o\sqrt{1-k^2s^2\psi} < 0 \qquad \text{(A-15)}$$

and*

$$t - t_n = -\frac{k}{\lambda\Omega_o}[F(k,\psi) - F(k,\psi_n)] \qquad \text{(A-16)}$$

where $\psi(t_n) \equiv \psi_n$, k is a positive constant to be specified* and

$$\lambda \equiv \sqrt{3\hat{K}} \qquad \text{(A-17)}$$

---

*The term $F(k,\psi)$ is an incomplete elliptic integral of the first kind tabulated[3] in terms of modulus k and argument ψ. When $\psi = n\pi/2$

$$F(k,n\pi/2) = nF(k,\pi/2) = nK(k)$$

where $K(k)$ is the complete elliptic integral of the first kind.

The time (T) for one revolution ($\psi = -2\pi+\psi_n$) relative to local vertical is

$$T = 2\pi/-\dot{\psi}_{ave} = 4kK(k)/\lambda\Omega_o \qquad \text{(A-18)}$$

Substituting for $\dot{\psi}_{ave}$ from Eq.(A-14) yields

$$(\pi/2)\lambda = kK(k) \qquad \text{(A-19)}$$

as the condition for Ψ to be periodic. An expression for Ψ in terms of ψ can be obtained from Eqs.(A-11) and (A-16)

$$\Psi = \psi + \Omega_o(t-t_n) = [\psi - \frac{k}{\lambda} F(k,\psi)] + \frac{k}{\lambda} F(k,\psi_n) \qquad \text{(A-20)}$$

Since the bracketed term is periodic with zero average value,* the nominal (or average) value of Ψ is

$$\Psi_N \equiv (k/\lambda) F(k,\psi_n) \qquad \text{(A-21)}$$

Consequently, the oscillation ($\Delta\Psi$) about Ψ_N is expressed by

$$\Delta\Psi \equiv \Psi-\Psi_N = \psi - (k/\lambda) F(k,\psi) \qquad \text{(A-22)}$$

The oscillation amplitude ($\Delta\Psi_m$) can be determined by examining the condition $\Delta\dot{\Psi} = \dot{\psi}+\Omega_o = 0$, which leads to

$$\Delta\Psi_m = \psi_m - (k/\lambda) F(k,\psi_m) \qquad \text{(A-23)}$$

where

$$\psi_m = \sin^{-1}\left(\sqrt{1/k^2-1/\lambda^2}\right) \qquad \text{(A-24)}$$

---

*Note that this term is zero whenever $\psi=n\pi/2$ and that it is an odd function in ψ. See Footnote *, (p. A-5) and Eq. (A-19).

Evaluation of $\Delta\Psi_m$ as a function of the parameter $\hat{K}$ follows after solving the transcendental equation (A-19) for k. A plot of $\Delta\Psi_m$ vs $|\hat{K}|$ is shown in Fig.(A-2).*

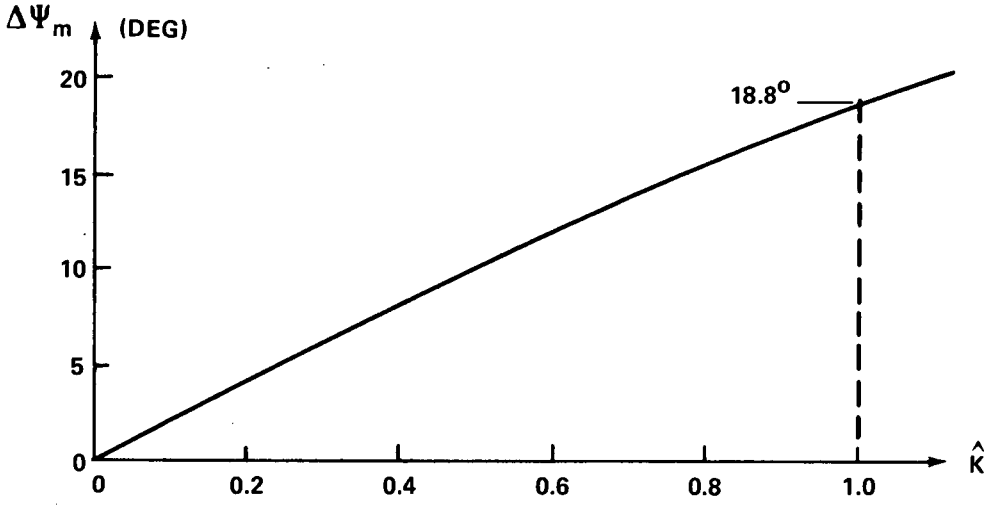

FIGURE A-2 - OSCILLATION AMPLITUDE IN THE QI MODE vs $\hat{K}$

As noted earlier the parameter $\hat{K}$ is arbitrary. Subsequently it will be shown that $\hat{K}$ can be chosen to minimize the control impulse requirement for maintaining the QI mode. Since $\hat{K}_{opt}$ usually falls within a range bounded by $|K_y|$ and $|K_z|$, which are always ≤ 1, only $|\hat{K}| \leq 1$ need be considered. For $\hat{K}=1$, the amplitude of oscillation is 18.8°. It should be observed that $\hat{K}=0$ corresponds to an inertial orientation** of the spacecraft (assuming $\dot{\psi}_o=0$).

A.2 Implementation of the QI Mode

Spacecraft attitude control systems frequently utilize a control law based on a linear combination of attitude and attitude rate errors for developing the control torque. Rate errors are generated simply by comparing

---

*The sign of $\hat{K}$ is immaterial since Eq.(A-12) remains the same if $\hat{K}$ and ψ are replaced by $-|\hat{K}|$ and $\psi+180°$ when $\hat{K}<0$.

**Inertial orientation is used loosely here, since the gradual motion of the orbital plane due to earth oblateness effects is ignored.

command rates ($\underline{\dot{\theta}}_c$) with vehicle rates ($\underline{\omega}$). Attitude errors may be developed differently, e.g., from inertial platform gimbal angle sensors or from strapped-down inertial navigation computations.[9,10] The latter method, which utilizes both command and vehicle rates, will be employed in the Skylab OA.[1]

In either case implementation of the QI mode requires specification of the command rate $\underline{\dot{\theta}}_c$. Since $\underline{\dot{\theta}}_c$ is a vector parallel to the orbit normal with magnitude $|\dot{\Psi}|$, it is given by

$$\underline{\dot{\theta}}_c^N = \begin{pmatrix} 0 \\ 0 \\ \dot{\Psi} \end{pmatrix} \tag{A-25}$$

in orbit referenced coordinates (x_N, y_N, z_N). (See Fig. (A-1)). From Eqs. (A-11) and (A-15) it follows that

$$\begin{aligned} \dot{\Psi} &= \dot{\psi} + \dot{\eta} = \dot{\psi} + \Omega_o \\ &= \Omega_o \left(1 - \frac{\lambda}{k}\sqrt{1-k^2 s^2 \psi}\right) \end{aligned} \tag{A-26}$$

It is necessary to compute ψ, the instantaneous angular displacement of x_p from the (upward) local vertical vector. This can be obtained by integrating Eq. (A-15) with an initial orientation $\psi(t_o) \equiv \psi_o$, which can be updated at intervals as desired.

A "tight" control loop and the command rate specication, $\underline{\dot{\theta}}_c$ will result in generating a control torque equivalent to $\underline{T}_c$ in Eq. (A-9) for a continuous controller (momentum exchange device or magnetic torquer) and a torque impulse equivalent to $\int_0^T |\underline{T}_c| dt$ for a discontinuous controller (reaction thrust system). Controller requirements for maintaining the mode are discussed in Appendix A.4 for a reaction thrust controller.

A.3 Initialization and Spacecraft Pointing Capability in the QI Mode

Initial conditions $(\Psi_o, \dot{\Psi}_o)$ for the x_p axis oscillation in the QI mode can be stated in terms of ψ_n since*

$$\Psi_o \equiv \Psi(t_n) = \psi_n + \eta_o = \psi_n \tag{A-26}$$

and

$$\dot{\Psi}_o \equiv \dot{\Psi}(t_n) = \dot{\psi}_n + \Omega_o = \Omega_o\left(1 - \frac{\lambda}{k}\sqrt{1-k^2s^2\psi_n}\right) \tag{A-27}$$

where $\dot{\psi}_n = \dot{\psi}(t_n)$ is obtained from Eq. (A-15).

The nominal orientation of the spacecraft in the QI mode can be specified, since Φ_o and Ψ_N, which is related to ψ_n by Eq.(A-21), are arbitrary. Consequently any spacecraft axis can be pointed arbitrarily in the celestial sphere and remain within a small neighborhood of the nominal orientation. It is straightforward to show that the angular displacement (δ) of some axis from its nominal orientation is given by

$$\delta = \cos^{-1}\left(c^2\gamma c(\Psi-\Psi_N) + s^2\gamma\right) \tag{A-28}$$

where γ is the latitude of the axis relative to the orbital plane. Since the respective latitudes of the y_p and z_p axes are defined by Φ_o and $90°-\Phi_o$, it follows that

$$\delta_{yp} = \cos^{-1}\left(c^2\Phi_o c(\Psi-\Psi_N) + s^2\Phi_o\right) \tag{A-29a}$$

and

$$\delta_{zp} = \cos^{-1}\left(s^2\Phi_o c(\Psi-\Psi_N) + c^2\Phi_o\right) \tag{A-29b}$$

---

*The motion may be initialized at times other than $t=t_n$ where $\psi=\psi_n$. See Section 5.3.

For any fixed Φ_o the maximum angular displacement occurs at $(\Psi-\Psi_N) = \Delta\Psi_m$, the oscillation amplitude. Thus,

$$\delta_{ym} \equiv \cos^{-1}(c^2\Phi_o c\Delta\Psi_m + s^2\Phi_o) \leq \Psi_m \qquad \text{(A-30a)}$$

$$\delta_{zm} \equiv \cos^{-1}(c^2\Phi_o + c\Delta\Psi_m s^2\Phi_o) \leq \Psi_m \qquad \text{(A-30b)}$$

These approach $\Delta\Psi_m$ as the particular axis nears the orbital plane. Plots of δ_{ym} and δ_{zm} vs Φ_o are shown in Fig.(A-3) for $\Delta\Psi_m = 16°$.

For the Skylab the nominal orientation is the solar inertial orientation shown in Fig.(A-4) in which x_p lies in the orbital plane and z_v (normal to solar array) is parallel to the sunline (inclined an angle β from the orbital plane*). The corresponding Φ_o and Ψ_N for this nominal orientation can be calculated with the help of Fig.(A-1) and the coordinate transformation

$$X_p = \begin{pmatrix} x_p \\ y_p \\ z_p \end{pmatrix} = \begin{bmatrix} \gamma_{11} & \gamma_{12} & \gamma_{13} \\ \gamma_{21} & \gamma_{22} & \gamma_{23} \\ \gamma_{31} & \gamma_{32} & \gamma_{33} \end{bmatrix} \begin{pmatrix} x_v \\ y_v \\ z_v \end{pmatrix} = [\gamma_{ij}]X_v \qquad \text{(A-31)}$$

relating principal and vehicle (geometric) axes. It can be shown that

$$\tan\Phi_o = \frac{-\gamma_{23}s\beta + \gamma_{33}\sqrt{c^2\beta-\gamma_{13}^2}}{-\gamma_{33}s\beta - \gamma_{23}\sqrt{c^2\beta-\gamma_{13}^2}} \qquad \text{(A-32)}$$

*Note: β (or $\eta_x^{(1)}$) is regarded positive when the sunline is below the orbital plane.

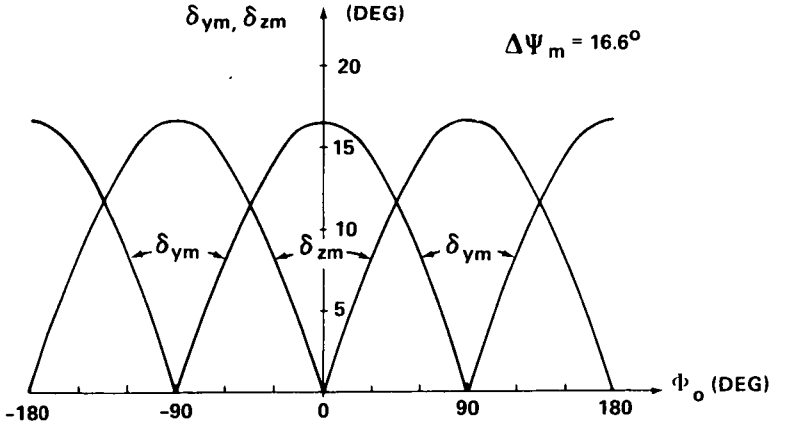

FIGURE A-3 - MAXIMUM INERTIAL POINTING DEVIATION vs Φ_o

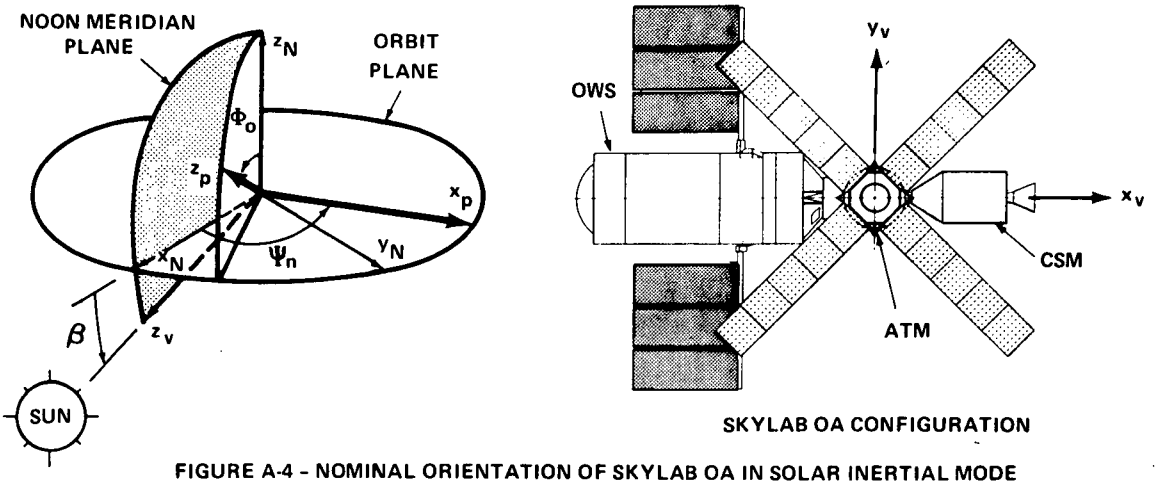

FIGURE A-4 - NOMINAL ORIENTATION OF SKYLAB OA IN SOLAR INERTIAL MODE

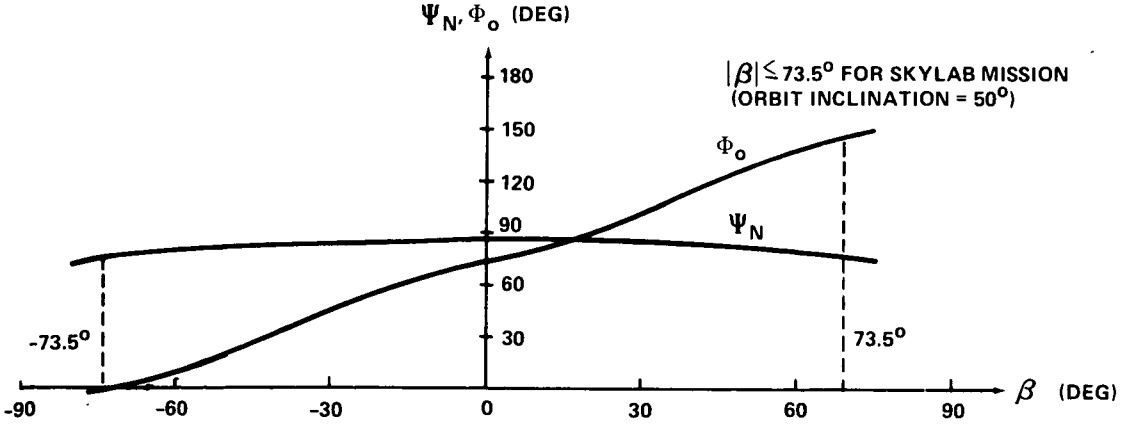

FIGURE A-5 - Φ_o AND Ψ_N vs β FOR NOMINAL SOLAR ORIENTATION

and $$\Psi_N = 90° + \eta_{tm} \tag{A-33}$$

where $$\eta_{tm} \equiv \sin^{-1}(\gamma_{13}/c\beta) \tag{A-34}$$

Curves of Φ_o and Ψ_N vs β based on Skylab mass properties data[4] for $[\gamma_{ij}]$ are shown in Fig. (A-5).

The maximum displacement (δ_{zvm}) of the Skylab z_v axis from the sunline (for any β) due to the oscillation (Ψ) can be evaluated from previous results. From Fig.(A-4) it follows that the latitude γ in Eq.(A-28) is $-\beta$ so that

$$\delta_{zv} = \cos^{-1}(c^2\beta c(\Psi-\Psi_N) + s^2\beta) \tag{A-35}$$

and

$$\delta_{zvm} = \cos^{-1}(c^2\beta c(\Delta\Psi_m) + s^2\beta) \leq \Delta\Psi_m \tag{A-36}$$

which indicates that δ_{zvm} is a maximum for $\beta=0°$ (viz. when z_V lies in the orbital plane).

A.4 Impulse Requirements for the QI Mode

Except for special cases ($I_z=I_y$ or $\Phi_o=\pm n\frac{\pi}{2}$, n=0,1,2) some control torque ($\underline{T}_c$) is required to sustain the QI mode. The purpose of this section is to select the parameter $\hat{K}$ so as to minimize the propellant requirements for a reaction thrust control system.

Propellant requirements are frequently stated in terms of the total force impulse (I_T) per orbit. This can be related to the total control torque impulse per orbit as follows

$$I_T = \frac{\int_0^T |T_{cx}^t|dt}{r_x} + \frac{\int_0^T |T_{cy}^t|dt}{r_y} + \frac{\int_0^T |T_{cz}^t|dt}{r_z} \tag{A-37}$$

Here T is the orbital period and (T_{cx}^t, T_{cy}^t, T_{cz}^t) are control torque components resolved along the effective thruster control axes (x_t, y_t, z_t). Also r_x, r_y and r_z are the magnitudes of the effective thruster lever arms relative to the spacecraft center of mass (CM).

For this analysis the geometric (x_v) and principal (x_p) axes are considered coincident* and the CM assumed to lie along the x_v axis. Also the thruster effective force directions are assumed to lie in a plane normal to the x_v axis as is the case for the OA/TACS and SM/RCS thrusters on Skylab A. However, the (y_v, z_v) geometric axes may be displaced by an angle ϕ_v from (y_p,z_p) and for slightly more generality the effective thruster axes (y_t,z_t) may be displaced by ϕ_c from (y_v,z_v) as on the CSM. (See Fig.(A-6)).

Based on the above discussion it follows that $r_y = r_z$ and

$$\underline{T}_c^t = \begin{pmatrix} T_{cx} \\ T_{cy} \\ T_{cz} \end{pmatrix}^t = \begin{pmatrix} T_{cx}^p \\ T_{cy}^p c\hat{\phi} + T_{cz}^p s\hat{\phi} \\ -T_{cy}^p s\hat{\phi} + T_{cz}^p c\hat{\phi} \end{pmatrix} \qquad \text{(A-38)}$$

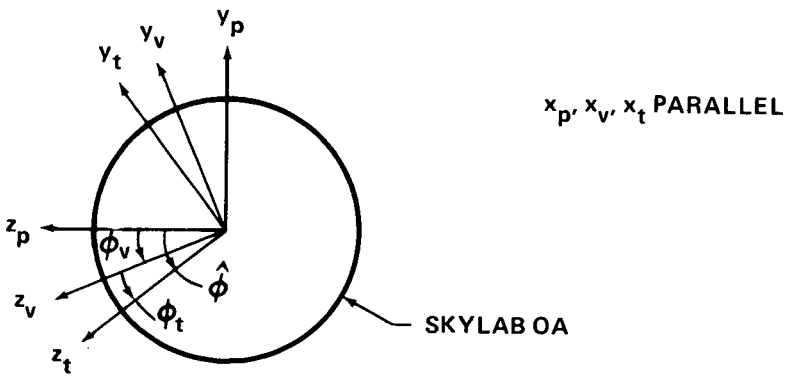

FIGURE A-6 - RELATIVE ORIENTATION OF PRINCIPAL, GEOMETRIC AND EFFECTIVE THRUSTER CONTROL AXES

*This is reasonable since x_v and x_p are within 4° for the Skylab OA.[4]

where $$\hat{\phi} \equiv \phi_v + \phi_c \tag{A-39}$$

consequently I_T may be expressed as

$$I_T = \frac{1}{r_x} (J_x + \hat{r} J_{yz}) \tag{A-40}$$

where

$$J_x \equiv \int_0^T |T_{cx}| dt \tag{A-41}$$

$$J_{yz} \equiv \int_0^T |T_{cy}^p c\hat{\phi} + T_{cz}^p s\hat{\phi}| dt + \int_0^T |-T_{cy}^p s\hat{\phi} + T_{cz}^p c\hat{\phi}| dt \tag{A-42}$$

and

$$\hat{r} \equiv r_x/r_y = r_x/r_z \tag{A-43}$$

Substitution of Eq. (A-9) for components of $\underline{T}_c^p$ yields

$$J_x = |T_{gmx} s2\Phi_o| \int_0^T \left| s^2(\Psi-\eta) + \frac{1}{3}(\dot{\Psi}/\Omega_o)^2 \right| dt \tag{A-44}$$

$$J_{yz} = \int_0^T \left| T_{gmx} \frac{s2(\Psi-\eta)}{\hat{k}} \left[(K_y - \hat{K}) \tilde{k} s\Phi_o c\hat{\phi} + (K_z - \hat{K}) c\Phi_o s\hat{\phi} \right] \right| dt$$

$$+ \int_0^T \left| T_{gmx} \frac{s2(\Psi-\eta)}{\hat{k}} \left[-(K_y - \hat{K}) \tilde{k} s\Phi_o s\hat{\phi} + (K_z - \hat{K}) c\Phi_o c\hat{\phi} \right] \right| dt$$

$$= |T_{gmx}| H(\hat{K}, \Phi_o, \hat{\phi}) \int_0^T |s2(\Psi-\eta)| dt \tag{A-45}$$

where

$$H(\hat{K}, \Phi_o, \hat{\phi}) \equiv \{ |B - A\hat{K}| + |D - C\hat{K}| \} / |\hat{k}| \tag{A-46}$$

$$\tilde{k} \equiv 1 - \hat{k} = I_y/I_z \tag{A-47}$$

and

$$A = c\Phi_o s\hat{\phi} + \tilde{k}s\Phi_o c\hat{\phi} \tag{A-48a}$$

$$B = K_z c\Phi_o s\hat{\phi} + \tilde{k}K_y s\Phi_o c\hat{\phi} \tag{A-48b}$$

$$C = c\Phi_o c\hat{\phi} - \tilde{k}s\Phi_o s\hat{\phi} \tag{A-48c}$$

$$D = K_z c\Phi_o c\hat{\phi} - \tilde{k}K_y s\Phi_o s\hat{\phi} \tag{A-48d}$$

An evaluation of the integrals in Eqs.(A-44) and (A-45) is given in Appendix D. With those results J_x and J_{yz} can be written as

$$J_x = \frac{T_{gmx}T}{2} \cdot F(\hat{K}) \left| s2\Phi_o \right| \tag{A-49}$$

$$J_{yz} = \frac{T_{gmx}T}{2} \cdot G(\hat{K})H(\hat{K}, \Phi_o, \hat{\phi}) \tag{A-50}$$

where

$$F(\hat{K}) = \frac{2}{3K(k)}\left\{\frac{3}{k^2}[K(k)-E(k)] + [(\lambda/k)^2 E[k]-K(k)]\right\} \tag{A-51}$$

$$G(\hat{K}) = 4\left(1 - \sqrt{1-k^2}\right)/k^2 K(k) \tag{A-52}$$

are implicit functions of $\hat{K}$ since k is related to $\hat{K}$ (or $\lambda = \sqrt{3\hat{K}}$) by Eq.(A-19), the oscillation condition.

Thus, the total impulse I_T may be written as

$$I_T = \frac{T_{gmx}T}{2r_x}[F(\hat{K}) \left| s2\Phi_o \right| + \hat{r}G(\hat{K})H(\hat{K}, \Phi_o, \hat{\phi})] \tag{A-53}$$

or in normalized form

$$NI_T = \frac{I_T}{I_{mx}} = F(\hat{K}) \left| s2\Phi_o \right| + \hat{r}G(\hat{K})H(\hat{K},\Phi_o,\hat{\phi}) \qquad (A\text{-}54)$$

where

$$I_{mx} \equiv \frac{T_{gmx}T}{2r_x} = \frac{h_{gmx}}{r_x} \qquad (A\text{-}55)$$

corresponds to the impulse per orbit required to cancel the maximum bias component of x axis gravity-gradient torque. Curves of $F(\hat{K})$ and $G(\hat{K})$ vs $\hat{K}$ are given in Fig.(A-7). A representative curve of $H(\hat{K},\Phi_o,\hat{\phi})$ is also shown for $\Phi_o=45°$, $\hat{\phi}=0°$ and Skylab data for inertia parameters K_z, K_y and $\hat{k}$. (See Appendix C.) Note that $F(0)$, $G(0)$ and $H(0,\Phi_o,\hat{\phi})$ correspond to an inertial orientation ($\hat{K}=0$).* The function $H(\hat{K},\Phi_o,\hat{\phi})$ generally has a relatively sharp minimum particularly when $\hat{k}$ is small, while $G(\hat{K})$ is relatively flat and $F(\hat{K})$ changes slowly with $\hat{K}$. Thus, minimization of NI_T with respect to $\hat{K}$ rests essentially on minimizing $H(\hat{K},\Phi_o,\hat{\phi})$.

A.4.1 Minimization with Respect to $\hat{K}$

From Eq.(A-46) it is evident that a plot of $H(\hat{K},\Phi_o,\hat{\phi})$ vs $\hat{K}$ consists of three linear segments as shown in Fig.(A-8). The minimum point occurs at one of the two corners

---

*The impulse I_T for an inertial orientation with $\hat{\phi}=0$ is given by

$$I_T = \left| \frac{T_{gmx}T}{2r_x} s2\Phi_o \right| + \left| \frac{T_{gmy}s\Phi_o}{r_y} \cdot \frac{4}{\Omega_o} \right| + \left| \frac{T_{gmz}c\Phi_o}{r_z} \frac{4}{\Omega_o} \right|$$

since $F(0)=1$, $G(0)=4/\pi$ and

$$H(0,\Phi_o,0) = \left| \frac{I_z-I_x}{I_z-I_y} s\Phi_o \right| + \left| \frac{I_y-I_x}{I_z-I_y} c\Phi_o \right|$$

defined by $\hat{K} = |B/A|$ and $\hat{K} = |D/C|$, that is

$$\bar{H}(\Phi_o, \hat{\phi}) \equiv \min_{\hat{K}} H(\hat{K}, \Phi_o, \hat{\phi}) = \begin{cases} \left|\frac{AD-BC}{A}\right| & |A| > |C| \\ \left|\frac{AD-BC}{C}\right| & |A| < |C| \end{cases} \qquad \text{(A-56)}$$

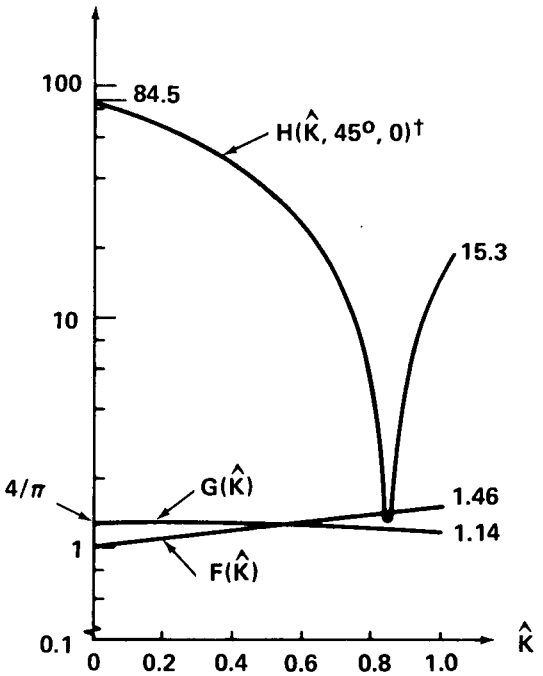

† SKYLAB INERTIA PARAMETERS

$K_z = 0.860$

$K_y = 0.834$

$\hat{k} = -.0143$

(See Appendix C)

FIGURE A-7 - IMPULSE PARAMETERS F, G, H vs $\hat{K}$

NOTE:
B/A < D/C
FOR ILLUSTRATION ONLY

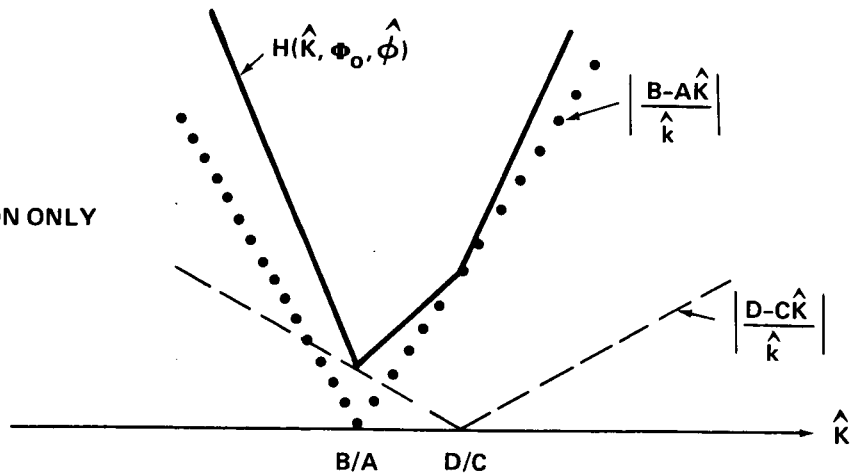

FIGURE A-8 - NATURE OF $H(\hat{K}, \Phi_o, \hat{\phi})$ NEAR A MINIMUM

Substitution for A, B, C and D from Eq.(A-48) and some manipulation yields

$$\bar{H}(\Phi_o,\hat{\phi}) = \begin{cases} \left|\frac{\tilde{k}}{2}\,\frac{(1+K_y)s2\Phi_o}{c\Phi_o s\hat{\phi} + \tilde{k}s\Phi_o c\hat{\phi}}\right| & |A|>|C| \\ \left|\frac{\tilde{k}}{2}\,\frac{(1+K_y)s2\Phi_o}{c\Phi_o c\hat{\phi} - \tilde{k}s\Phi_o s\hat{\phi}}\right| & |A|<|C| \end{cases} \qquad \text{(A-57)}$$

and

$$\hat{K}_{opt} \equiv \begin{cases} \left|\frac{B}{A}\right| = \dfrac{K_z c\Phi_o s\hat{\phi} + \tilde{k}K_y s\Phi_o c\hat{\phi}}{c\Phi_o s\hat{\phi} + \tilde{k}s\Phi_o c\hat{\phi}} & |A|>|C| \\ \left|\frac{D}{C}\right| = \dfrac{K_z c\Phi_o c\hat{\phi} - \tilde{k}K_y s\Phi_o s\hat{\phi}}{c\Phi_o c\hat{\phi} - \tilde{k}s\Phi_o s\hat{\phi}} & |A|<|C| \end{cases} \qquad \text{(A-58)}$$

The normalized impulse for $\hat{K}=\hat{K}_{opt}$ may be evaluated from Eqs.(A-51, 52, 54, 57 and 58) as

$$\overline{NI}_T = F(\hat{K}_{opt})\,|s2\Phi_o| + \hat{r}G(\hat{K}_{opt})\bar{H}(\Phi_o,\hat{\phi}) \qquad \text{(A-59)}$$

The condition $|A|\geq|C|$ implies that

$$\tilde{k}s2\Phi_o s2\hat{\phi} \geq c2\hat{\phi}(c^2\Phi_o - \tilde{k}^2 s^2\Phi_o) \qquad \text{(A-60)}$$

For equality it follows that

$$\hat{\phi} = \pm\frac{n\pi}{4} + \tan^{-1}\left(\frac{1}{\tilde{k}\,\tan\Phi_o}\right) \qquad n=1,3,5.... \qquad \text{(A-61)}$$

Regions in the $(\hat{\phi},\Phi_o)$ plane where the cases, $|A|>|C|$ or $|A|<|C|$, apply, are shown in Fig.(A-9). The boundaries corresponding to Eq.(A-61) are based on Skylab inertia parameters, so that $\tilde{k} = 1.0143$ (See Appendix C).

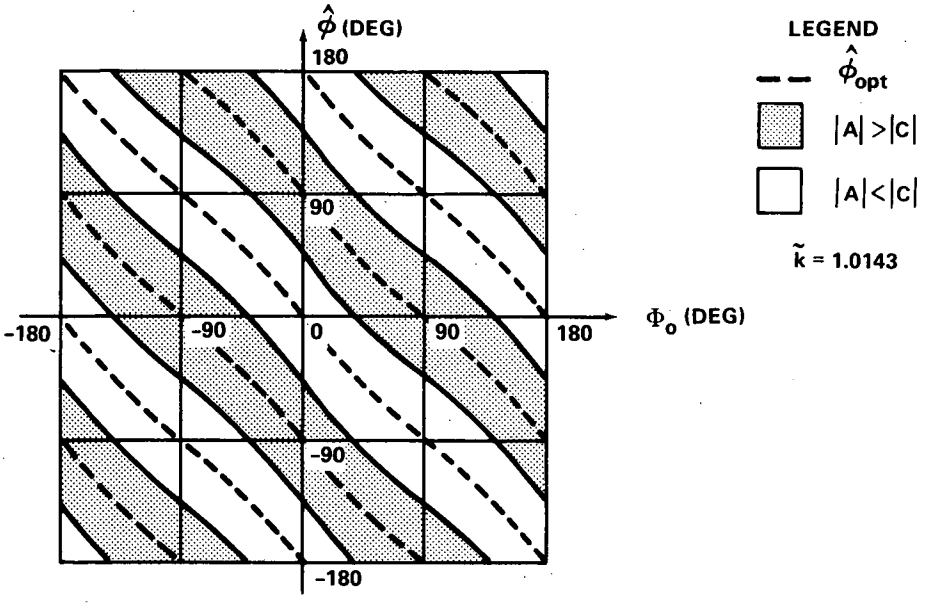

FIGURE A-9 - REGIONS FOR $|A|>|C|$ AND $|A|<|C|$ IN $(\hat{\phi}, \Phi_o)$ PLANE

A.4.2 Minimization with Respect to $\hat{\phi}$

To assess the impact of thruster control axis displacement $(\hat{\phi})$ from the principal axes, $\bar{H}(\Phi_o,\hat{\phi})$ can be minimized to determine the optimal $\hat{\phi}$ for any given Φ_o. Thus, $\partial\bar{H}(\Phi_o,\hat{\phi})/\partial\hat{\phi} = 0$ yields

$$\hat{\phi}_{opt} = \begin{cases} \tan^{-1}(1/\tilde{k}\,\tan\Phi_o) & |A|>|C| \\ \tan^{-1}(-\tilde{k}\,\tan\Phi_o) & |A|<|C| \end{cases} \qquad \text{(A-62)}$$

Comparing this result with Eq.(A-61) indicates that the loci, $\hat{\phi}_{opt}$ vs Φ_o, lie midway (i.e., $\pm 45°$) between boundaries of the respective regions, $|A|>|C|$ and $|A|<|C|$, in Fig.(A-9).

Substitution of $\hat{\phi}_{opt}$ for $\hat{\phi}$ in Eqs.(A-57) and (A-58) yields

$$\bar{\bar{H}}(\Phi_o) \equiv \min_{\hat{\phi}} \bar{H}(\Phi_o,\hat{\phi}) = \left| \frac{\tilde{k}(1+K_y)s2\Phi_o}{2\sqrt{c^2\Phi_o + \tilde{k}^2 s^2\Phi_o}} \right| \qquad (A\text{-}63)$$

and

$$\bar{\bar{K}}_{opt} \equiv \hat{K}_{opt}(\Phi_o,\hat{\phi}_{opt}) = \left| \frac{K_z c^2\Phi_o + \tilde{k}^2 K_y s^2\Phi_o}{c^2\Phi_o + \tilde{k}^2 s^2\Phi_o} \right| \qquad (A\text{-}64)$$

for both cases. The normalized impulse is thus

$$\bar{\bar{\overline{NI}}}_T = |s2\Phi_o| \left[F(\hat{K}_{opt}) + \hat{r}G(\hat{K}_{opt}) \frac{|\tilde{k}|(1+K_y)}{2\sqrt{c^2\Phi_o + \tilde{k}^2 s^2\Phi_o}} \right] \qquad (A\text{-}65)$$

A plot of $\bar{\bar{\overline{NI}}}_T$ and $\bar{\bar{K}}_{opt}$ vs Φ_o is shown in Fig.(A-10) for Skylab inertia parameters $(K_z,K_y,\tilde{k})$ and three values of $\hat{r}$. It can be observed that

$$K_y \leq \bar{\bar{K}}_{opt} \leq K_z \qquad (A\text{-}66)$$

From Eq.(A-64) it follows that $\bar{\bar{K}}_{opt}$ always lies between $|K_y|$ and $|K_z|$ if x_p is a principal axis of maximum or minimum moment of inertia (i.e. K_y,K_z have the same algebraic sign).

A.4.3 Comparison of Results

The relative effect of $\hat{\phi}$ on impulse requirements can be assessed from the ratio

$$\mu = \overline{NI}_T / \bar{\bar{\overline{NI}}}_T \qquad (A\text{-}67)$$

where $\overline{NI}_T$ and $\overline{\overline{NI}}_T$ are defined by Eqs.(A-59) and (A-65). Curves of μ vs $|\Phi_o|$ based on Skylab inertia parameters and $\hat{r}$=0.25 are shown in Fig.(A-11a) for various $|\hat{\phi}|$. It can be seen in Fig.(A-11b) that the $\hat{K}_{opt}$ corresponding to $\overline{NI}_T$ remain within or very close to the interval $K_y \leq \hat{K} \leq K_z$. It is clear that $\hat{\phi}$ has a 6% effect, at most, on the impulse requirements for $\hat{K}_{opt}$ in this range. The effect would increase however, for $\hat{r}$>0.25.

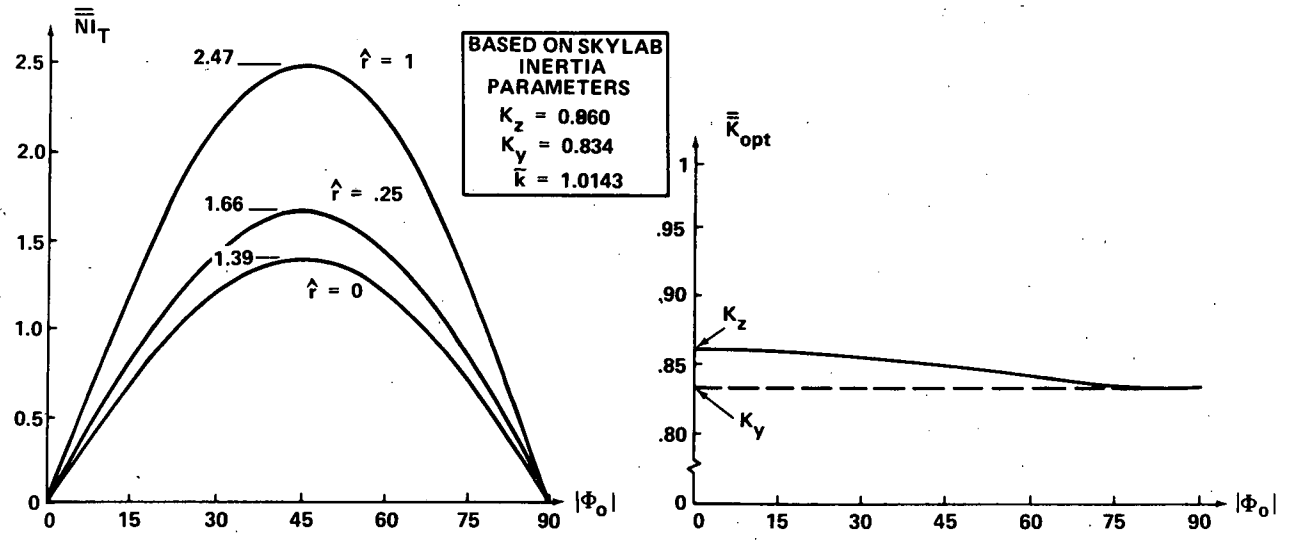

FIGURE A-10 - $\overline{\overline{NI}}_T$ AND $\bar{\bar{K}}_{opt}$ vs Φ_o

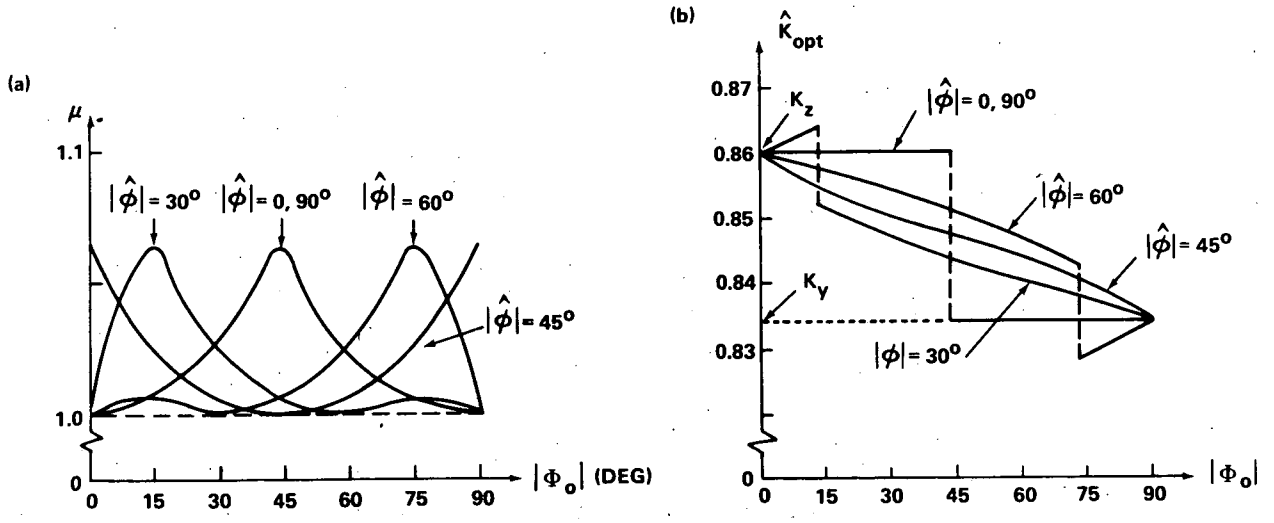

FIGURE A-11 - μ AND $\hat{K}_{opt}$ vs Φ_o

APPENDIX B

Evaluation of Integrals

The purpose of this Appendix is to evaluate two integrals encountered in determining the propellant impulse requirements for reaction thrust control of spacecraft in the QI mode. These were stated in Eqs. (A-44) and (A-45) as

$$J_x = |T_{gmx} s2\Phi_o| \int_o^T |s^2(\Psi-\eta) + \tfrac{1}{3}(\dot{\Psi}/\Omega_o)^2| dt \tag{B-1}$$

and

$$J_{yz} = |T_{gmx}| H(\hat{K}, \Phi_o, \hat{\phi}) \int_o^T |s^2(\Psi-\eta)| dt \tag{B-2}$$

The problem can be converted to an integration with respect to the variable ψ by using Eqs. (A-11), (A-15) and (A-16) and noting that

$$dt = \frac{d\psi}{\dot{\psi}} = \frac{d\psi}{-\Omega_o (\lambda/k) M} = \frac{T}{2} \frac{-d\psi}{(\pi\lambda/k) M} \tag{B-3}$$

where

$$M \equiv \sqrt{1-k^2 s^2 \psi} \tag{B-4}$$

and $\Omega_o = 2\pi/T$. This yields

$$J_x = \left| \frac{T_{gmx}\, T}{2} s2\Phi_o \right| F(\hat{K}) \tag{B-5}$$

and

$$J_{yz} = \left| \frac{T_{gmx}\, T}{2} \right| H(\hat{K}, \Phi_o, \hat{\phi}) G(\hat{K}) \tag{B-6}$$

where

$$F(\hat{K}) \equiv \frac{-k}{\pi\lambda}\int_{o}^{-2\pi} \left| s^2\psi + \frac{1}{3}(1-\lambda M/k)^2 \right| d\psi/M \qquad \text{(B-7)}$$

and

$$G(\hat{K}) \equiv \frac{-k}{\pi\lambda}\int_{o}^{-2\pi} \left| s^2\psi \right| d\psi/M \qquad \text{(B-8)}$$

The limits $(0,-2\pi)$ are based on $\psi_o=0$ for convenience. This has no effect on the desired result, since the integration is over an entire orbital period. The terms F and G are a function of the oscillation parameter, $\hat{K}$, since k is related to $\hat{K}$ by Eqs. (A-17) and (A-19).

B.1 $\underline{F(\hat{K})}$

The integrand in Eq. (B-7) is always positive and independent of the algebraic sign of ψ. Hence

$$F(\hat{K}) = \frac{4}{\pi(\lambda/k)}\int_{0}^{\pi/2}\left\{ s^2\psi + \frac{1}{3}[1-\lambda M/k]^2 \right\} d\psi/M$$

$$= \frac{4}{\pi(\lambda/k)}\left\{ \frac{1}{k^2}\int_{0}^{\pi/2}\left(\frac{1}{M} - M\right)d\psi + \frac{1}{3}\int_{0}^{\pi/2}\frac{d\psi}{M} - \frac{2\lambda}{3k}\int_{0}^{\pi/2} d\psi + \frac{\lambda^2}{3k^2}\int_{0}^{\pi/2} M d\psi \right\} \qquad \text{(B-9}$$

The terms involving M are all in the standard form of complete elliptic integrals of the first or second kinds[3] so that

$$F(\hat{K}) = \frac{4}{\pi(\lambda/k)}\left\{ \frac{1}{k^2}\left[K(k)-E(k)\right] + \frac{1}{3}\left[K(k) - 2\cdot\frac{\pi\lambda}{2k} + \frac{\lambda^2}{k^2}E(k)\right] \right\} \qquad \text{(B-10)}$$

Making use of Eq. (A-19), the oscillation condition, yields

$$F(\hat{K}) = \frac{2}{3K(k)} \left\{ \left(\frac{3}{k^2} - 1\right) K(k) + \left(\frac{\lambda^2 - 3}{k^2}\right) E(k) \right\} \tag{B-11}$$

B.2 $\underline{G(\hat{K})}$

The integrand in Eq. (B-8) retains the same algebraic sign over any quarter period of ψ. Hence,

$$G(\hat{K}) = \frac{-4}{\pi(\lambda/k)} \int_0^{-\pi/2} (-s^2\psi) \frac{d\psi}{M} = \frac{4}{\pi(\lambda/k)} \int_0^{\pi/2} \frac{s^2\psi}{M} d\psi$$

$$= \frac{4}{(\pi\lambda/2k)} \left(\frac{1-\sqrt{1-k^2}}{k^2} \right) = \frac{4(1-\sqrt{1-k^2})}{k^2 \; K(k)} \tag{B-12}$$

APPENDIX C

Spacecraft Inertia Parameters

The manipulation and interpretation of mathematical relationships in rotational dynamics is often facilitated by introducing the following parameters expressed in terms of spacecraft principal axis inertias (I_x, I_y, I_z).

$$K_x \equiv \frac{I_z - I_y}{I_x} = \frac{K_y - K_z}{1 - K_y K_z} \tag{C-1}$$

$$K_y \equiv \frac{I_z - I_x}{I_y} = \frac{K_z + K_x}{1 - K_x K_z} \tag{C-2}$$

$$K_z \equiv \frac{I_y - I_x}{I_z} = \frac{K_y - K_x}{1 - K_x K_y} \tag{C-3}$$

Since $I_i \leq I_j + I_k$ $(i,j,k = x,y \text{ or } z)$, it follows that K_x, K_y and K_z lie in the interval

$$0 \leq |K_i| \leq 1 \qquad (i = x,y,z) \tag{C-4}$$

Note that any K_i can be expressed in terms of the other two parameters (K_j, K_k).

The relationship of K_z to K_x and K_y is shown on the (K_x, K_y) plane in Fig. (C-1). A given spacecraft is represented by a point on this plane. Shading indicates regions, where the spacecraft x axis corresponds to an axis of minimum moment of inertia (Region A), intermediate moment of inertia (Region B) or maximum moment of inertia (Region C).

Additional identities useful in the foregoing analyses are

$$\hat{k} \equiv (I_z - I_y)/I_z \tag{C-5}$$

$$\tilde{k} \equiv I_y/I_z = 1 - \hat{k} \tag{C-6}$$

$$(K_z - K_y) = -\hat{k}(1 + K_y) \tag{C-7}$$

Numerical values of the inertia parameters corresponding to the Skylab OA configuration are given in Table C-1. The corresponding point on the (K_x, K_y) plane is noted in Fig. (C-1).

TABLE C-1

INERTIA PARAMETERS FOR SKYLAB OA

PRINCIPAL AXIS INERTIAS (SLUG-FT^2)†	K_x	K_y	K_z	$\hat{k}$	$\tilde{k}$
$I_x = 0.6536 \times 10^6$ $I_y = 4.3039 \times 10^6$ $I_z = 4.2433 \times 10^6$	- .093	0.834	0.860	- .0143	1.0143

†BASED ON DATA FROM REFERENCE (4)

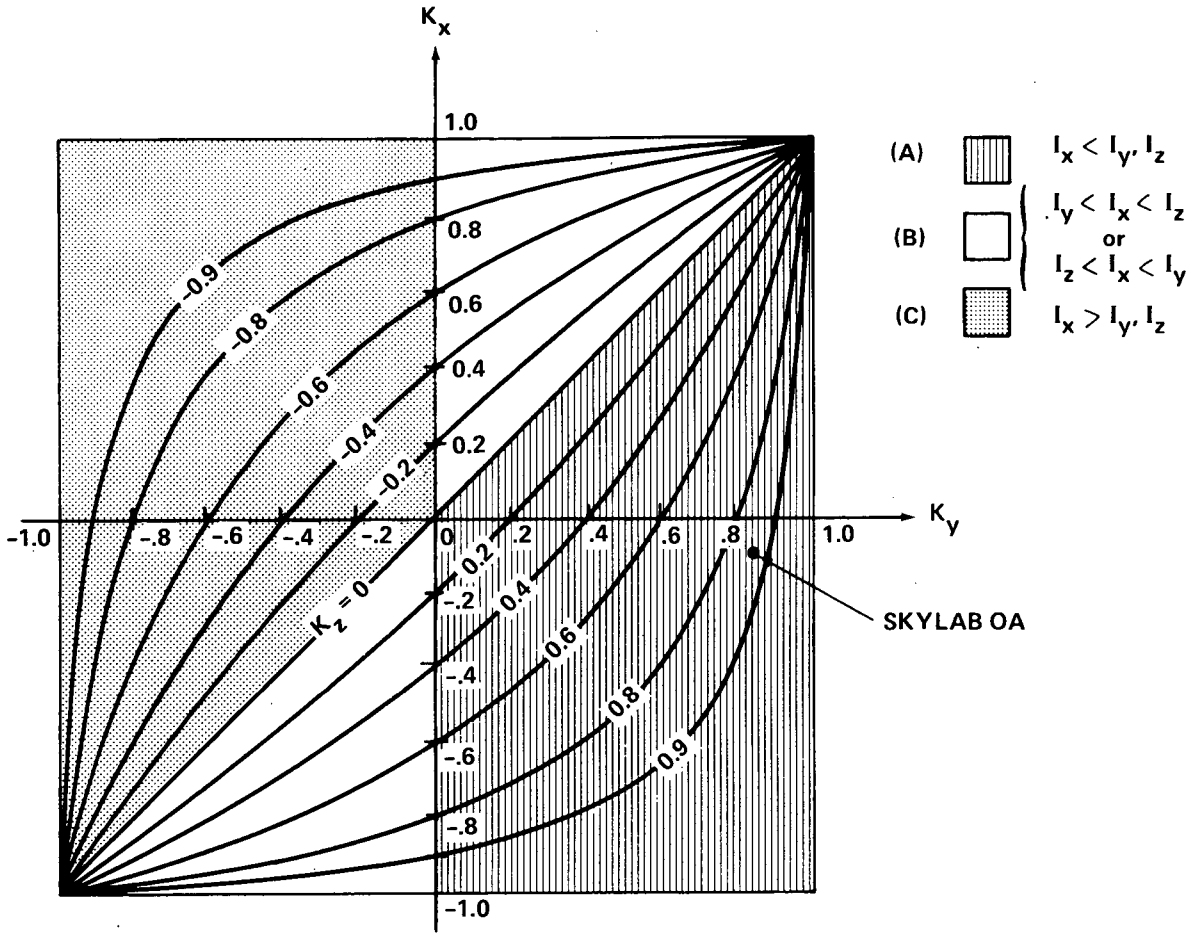

FIGURE C-1 - (K_x, K_y) INERTIA PARAMETER PLANE

Appendix D

Summary of Equations for Generating QI Mode Command Rate

A sequence of computations for generating the command rate $\dot{\Psi}$ is stated below. Corresponding equation numbers in the preceding text are noted at each step for the various parameters. Known data are assumed to be:

I_x, I_y, I_z - spacecraft principal axis inertias

$[\gamma_{ij}]$ - direction cosine matrix relating principal and geometric coordinates ($X_p = [\gamma_{ij}] X_v$)

Ω_o - mean orbit angular velocity

$\eta(t_j)$ - orbital position relative to orbital noon at time, t_j

β - angle between sunline and orbital plane (positive with sunline below orbital plane)

Fixed Parameter Calculations*

(C-2) $$K_y = (I_z - I_x)/I_y \qquad \text{(D-1)}$$

(C-3) $$K_z = (I_y - I_x)/I_z \qquad \text{(D-2)}$$

(A-32) $$\Phi_o = \tan^{-1}\left[\frac{-\gamma_{23}s\beta + \gamma_{33}\sqrt{c^2\beta - \gamma_{13}^2}}{-\gamma_{33}s\beta - \gamma_{23}\sqrt{c^2\beta - \gamma_{13}^2}}\right] \qquad \text{(D-3)}$$

(18) $$\hat{K} = K_z c^2\Phi_o + K_y s^2\Phi_o \qquad \text{(D-4)}$$

---

*These parameters may be re-evaluated at intervals to account for changes in Ω_o, β and the mass characteristics: I_x, I_y, I_z and $[\gamma_{ij}]$.

$$\lambda = \sqrt{3\hat{K}} \tag{D-5}$$

(8) $$(\pi/2)\ \lambda = kK(k) \qquad \text{(solve iteratively for k)} \tag{D-6}$$

(A-34) $$\eta_{tm} = \sin^{-1}\ (\gamma_{13}/c\beta) \tag{D-7}$$

(28) $$\eta_p = \eta_{tm} + (p-2)\pi/2 \qquad p = 1,2,3,4 \tag{D-8}$$

(11) $$\psi_m = \sin^{-1}\sqrt{1/k^2 - 1/\lambda^2} \tag{D-9}$$

(10) $$\Delta\Psi_m = \psi_m - (k/\lambda)F(k,\psi_m) \tag{D-10}$$

ψ Initialization or Update Calculations

(34) $$\psi(t_j) = (3-p)\pi/2 + (\lambda/k)[\eta(t_j)-\eta_p]$$

$$|\eta(t_j)-\eta_p| < 18° \qquad p = 1,3 \tag{D-11}$$

or*

(36) $$\psi(t_j) \simeq \pi/2 - \{-\Delta\Psi_m \sin 2[\eta(t_j)-\eta_{tm}] + [\eta(t_j)-\eta_{tm}]\}$$

$$\text{all } \eta(t_j) \tag{D-12}$$

$\dot{\psi}$ Integration

(12) $$\dot{\psi}(\tau) = -\Omega_o(\lambda/k)\sqrt{1-k^2s^2\psi(\tau)} \qquad t_j \leq \tau \leq t_{j+1} \tag{D-13,}$$

---

*This expression is exact for $\eta(t_j) = \eta_p$ $(p = 1,2,3,4)$. The error is at most 1.3° for any $\eta(t_j)$.

$\dot{\Psi}$ Calculation

(6) $$\dot{\Psi}(t_{j+1}) = \dot{\psi}(t_{j+1}) + \Omega_o \qquad \text{(D-14a)}$$

$$= \Omega_o \left[1 - (\lambda/k) \sqrt{1-k^2 s^2 \psi(t_{j+1})} \right] \qquad \text{(D-14b)}$$

The result in Eq. (D-14a) is useful if $\dot{\psi}(t_{j+1})$ is determined by integrating Eq. (D-13) with Eq. (D-11) as the initial condition. The result in Eq. (D-14b) is useful if $\psi(t_{j+1})$ is determined from Eq. (D-12) with t_j replaced by t_{j+1}.

The command rate vector $\underline{\dot{\Theta}}_C$ is parallel to the orbit normal with magnitude $|\dot{\Psi}|$. It must be resolved into an appropriate coordinate system for use with either OA/TACS or SM/RCS control.

Appendix E

List of Symbols and Abbreviations

This list defines major symbols appearing throughout the memorandum. Minor symbols or symbols appearing in only one section are omitted.

Greek Symbols	Definition
β	angle between sun line and orbital plane (positive with sun line below orbital plane)
δ_{zv}	angle between Skylab z geometric axis (z_v) and sun line
η	angular displacement from orbital noon (orbit position)
η_p	η when $\psi = (3-p)\pi/2$ $(p = 1,2,3,4)$
η_{tm}	orbit angle offset of x_p from normal to the sun-line in the SI orientation (due to displacement of x_p and x_v)
λ	$\sqrt{3\hat{K}}$
$\hat{\phi}$	angular displacement (about x_v) between transverse principal and thruster control axes. (See Figure 8)
ψ	instantaneous angular displacement of x_p from (upward) local vertical in QI mode
$\dot{\psi}, \ddot{\psi}$	$d\psi/dt$, $d^2\psi/dt^2$
ψ_m	parameter used in evaluating ψ when $\Delta\Psi = \pm\Delta\Psi_m$
ψ_n	ψ when $t = t_n$
ψ_o	ψ at some initial or re-initialization time t_o.

Greek Symbols	Definition
$\Delta\Psi$	instantaneous angular displacement of x_p from nominal in QI mode ($\Delta\Psi = \Psi - \Psi_N$)
$\Delta\dot{\Psi}$	$d(\Delta\Psi)/dt$
$\Delta\Psi_m$	amplitude of oscillation in QI mode
$\underline{\dot{\Theta}}_c$	command rate vector in QI mode: $\underline{\dot{\Theta}}_c = (0\ 0\ \dot{\Psi})^T$ in (x_N, y_N, z_N) coordinates
Φ_o	angular displacement (about x_p) of z_p from orbit normal (z_N) such that z_v points to sun in the SI orientation. See Figure (A-4).
Ψ	instantaneous angular displacement of x_p from x_N in QI mode
$\dot{\Psi}, \ddot{\Psi}$	$d\dot{\Psi}/dt$, $d^2\Psi/dt^2$
$\dot{\Psi}_{ave}$	average value of $\dot{\Psi}$ over an orbit
Ψ_N	nominal value of Ψ ($\Psi_N = \pi/2 + \eta_{tm}$)
Ω_o	mean orbit angular velocity
English Symbols	
k	parameter in QI motion equations (chosen such that $\dot{\psi}_{ave} = -\Omega_o$)
$\hat{k}, \tilde{k}$	spacecraft inertia parameters (see Appendix C)
$\hat{r}$	r_x/r_{yz}
r_x	effective thruster lever arm (x axis)
r_{yz}	effective thruster lever arm (y and z axes)
$(t-t_n)$	elapsed time since last orbital noon
t	absolute time (e.g. GMT since SL-1 launch)

English Symbols	Definition
t_n	absolute time of last orbital noon
(x_N, y_N, z_N)	orbital coordinates (z_N - normal to orbital plane, x_N - noon upward local vertical)
(x_p, y_p, z_p)	OA principal coordinates (displaced 180° about x_p from Reference 4 principal axes)
(x_v, y_v, z_v)	OA geometric coordinates (vehicle coordinates in Reference 1)
A_0	attitude error gain control in thruster control law (deadband = $\pm 1/A_0$)
A_1	rate error gain constant in thruster control law (switch-line slope = $-A_0/A_1$)
$E(k)$	complete elliptic integral of second kind (modulus, k)
$F(k,\psi)$	incomplete elliptic integral of first kind (modulus, k; argument, ψ)
I_x, I_y, I_z	OA principal axis inertias
I_T	theoretical impulse per orbit required to counteract gravity gradient torque in QI mode
I_{mx}	impulse per orbit required to counteract bias component of x axis gravity gradient torque in QI modes for $\lvert\Phi_o\rvert$ = 45° or 135°.
$\hat{K}$	arbitrary parameter in QI motion equations
$\hat{K}_{opt}$	optimal value of $\hat{K}$ (chosen to minimize I_T)
$K(k)$	complete elliptic integral of the first kind (modulus, k)
K_y, K_z	spacecraft inertia parameters (see Appendix C)
NI_T	I_T/I_{mx} (normalized impulse per orbit)
T	orbital period ($T = 2\pi/\Omega_o$)
T_{gmx}	maximum gravity gradient torque on x_p axis; $3\Omega_o^2(I_z-I_y)/2$

Abbreviations	Definition
ATM	Apollo Telescope Mount
ATMDC	Apollo Telescope Mount Digital Computer
CMC	Command Module Computer
CMG	Control Moment Gyro
CSM	Command & Service Module
CSM/DAP	CSM Digital Auto-Pilot
IMU	Inertial Measurement Unit (Inertial Platform)
OA	Orbital Assembly (CSM + SWS)
QI	Quasi-Inertial
SI	Solar-Inertial
SL-2,SL-3,SL-4	CSM#1, CSM#2, CSM#3 in Skylab Mission
SM/RCS	Service Module Reaction Control System
SWS	Saturn Workshop (also SL-1)
OA/TACS	OA Thruster Attitude Control System
WDB	Wide Deadband

References

1. "ATMDC Program Definition Document (PDD)", Part I, IBM (Huntsville) Report No. 70-207-0002, November 4, 1970.

2. B. D. Elrod, "Quasi-Inertial Stabilization of the AAP-1/ AAP-2 Cluster Configuration", Bellcomm Technical Report, TR-67-600-3-1, April 14, 1967.

3. E. Jahnke and F. Emde, "Tables of Functions", 4th Ed., Dover Publications, New York, N.Y., 1945, pp. 52-89.

4. "Skylab A Mass Properties", MSFC Memorandum, S&E-ASTN-SAE-70-40, Table IV, Event 6, June 18, 1970.

5. "Skylab Program Operational Data Book", Vol. II - Mission Mass Properties, Vol. III - CSM Performance Data, Vol. IV - Skylab 1 Performance Data, MSC Document (MSC-01549), February 1970.

6. "Propulsion System Consumables Analysis for the Preliminary Reference Skylab Flight Plan (SL-1/2 Mission)", MSC Internal Note No. 71-FM-53, February 4, 1971.

7. D. D. Nixon and H. E. Worley, "Release of the Roll Deadband to Reduce WACS Propellant Consumption for the X-POP Inertial Fixed Mode of the OWS", MSFC Report S&E-AERO-DOI-4-69, June 12, 1969.

8. J. J. Fearnsides, "An Evaluation of Various Strategies for Implementing a Minimum Fuel, Attitude Hold Control Mode for the AAP Orbital Workshop", Bellcomm Technical Memorandum TM-69-1022-10, September 30, 1969.

9. J. C. Wilcox, "A New Algorithm for Strapped - Down Inertial Navigation", IEEE Transactions on Aerospace & Electronic Systems, September 1967, pp. 796-802.

10. B. D. Elrod, "A Quaternion Differential Equation for Spacecraft Attitude Error", Bellcomm Memorandum for File B70 10066, October 30, 1970.

11. T. J. Smith, "Equations for Quasi-Inertial Backup Attitude Hold", TRW Systems - Electronics Laboratory Report 17618-M127-R0-00, April 23, 1971.

12. J. E. Johnson, "Orbital Aerodynamic Data for the Skylab Cluster Configuration with and without the Docked CSM", MSFC Report S&E-AERO-AA-70-21, March 23, 1970.